Title:

Proteomic analysis to classify extracellular vesicles and plasmodesmata in Arabidopsis cell culture supernatants

Takehito Takei[1], Teppei Asou[1], Nobuteru Hamakawa[1], Ryo Noguchi[1], Kohei Sumiyoshi[2], Kenji Sueyoshi[3], Koshi Imami[4], Takahiro Hamada[1]

1. Department of Bioscience, Faculty of Life Science, Okayama University of Science, Ridaicho 1-1, Okayama, 700-0005, Japan
2. Department of Applied Chemistry, Graduate School of Engineering, Osaka Metropolitan University, Osaka, 599-8531, Japan
3. Department of Chemistry, School of Science, Kitasato University, Sagamihara, Kanagawa, 252–0373, Japan
4. Proteome Homeostasis Research Unit, RIKEN Center for Integrative Medical Sciences, Tsurumi-ku, Yokohama, Kanagawa 230-0045, Japan

Corresponding author e-mail:
hama.micro@ous.ac.jp

Short title: Arabidopsis PD and EV proteomes

Abstract

The plant apoplast contains diverse proteins. In this study, we analyzed the extracellular vesicle (EV) proteome using cell culture supernatants. Unexpectedly, many plasmodesmata proteins were identified. The comparison between the cell culture EV proteome and the plasmodesmata proteome revealed that EV and plasmodesmata proteins were indistinguishable. Highly sensitive imaging analyses showed that PDLP3, a representative plasmodesmata marker, was localized to plasmodesmata, but it was also present as small granules in apoplast regions. The small PDLP3 granules were similar in size to the EVs, implying that the PDLPs identified during the proteomic analysis may be small PDLP granules secreted into apoplast regions, rather than proteins derived from the plasmodesmata itself. Next, we attempted to distinguish EV proteins from plasmodesmata proteins. The step-wise density gradient ultracentrifugation and clustering analysis separated EV protein clusters (represented by tetraspanins and membrane trafficking proteins) from plasmodesmata clusters (represented by PDLPs and PDCBs). These results provide the basis for future explorations of plant plasmodesmata and EVs.

41 **Introduction**

42 Plant extracellular vesicles (EVs) are mainly secreted from multi-vesicular bodies
43 (MVBs) generated in the endoplasmic reticulum (ER) via Golgi bodies and the trans-
44 Golgi network (TGN) pathway (Gao et al., 2017a; Otegui, 2018). Multi-vesicular bodies
45 also affect degradation pathways by transporting proteins and lipids to vacuoles. For
46 example, proteins ubiquitinated in the plasma membrane are transported to MVBs via
47 endocytosis, after which the MVBs fuse to the vacuolar membrane (Mosesso et al., 2019).
48 Different SNAREs and Rab GTPases contribute to the fusion of MVBs to the plasma and
49 vacuolar membranes (Ito and Uemura, 2022). For example, ARA6, VAMP721/VAMP722,
50 and SYP121/SYP122 mediate the fusion of MVBs to the plasma membrane, whereas
51 ARA7/RHA1 and VAMP727 participate in the fusion of MVBs to the vacuolar membrane.

52 However, EVs are not only derived from MVBs, suggestive of a relatively complex
53 process. The secretion of EVs is activated in plants infected by pathogenic fungi and
54 bacteria (Wang et al., 2017; Hansen and Nielsen, 2017). During an infection by
55 pathogenic fungi, vacuolar and plasma membranes fuse together, which leads to the
56 extracellular secretion of vacuolar components, including MVB-derived vesicles and
57 autophagosomes (Cui et al., 2020). Although *Arabidopsis thaliana* (Arabidopsis) plants
58 are normally resistant to *Golovinomyces orontii*, a mutation to *PEN1* (*SYP121*) results in
59 plants that are susceptible to this phytopathogenic fungus that causes powdery mildew
60 (Collins et al., 2003; Assaad et al., 2004; Lipka et al., 2005). The *SYP121* gene encodes a
61 SNARE protein involved in fusing membranes, suggesting it contributes to the secretion
62 of EVs. However, SYP121 was also detected in EVs, implying it may not be involved in
63 the fusion of MVBs to the plasma membrane (Meyer et al., 2009; Nielsen and Thordal-
64 Christensen, 2012). These findings reflect the importance of membrane trafficking factors

65 for plant responses to disease, but the precise functions of SYP121 on plant resistance to
66 phytopathogenic fungi remain unclear.
67
68 Identifying the contents of purified EVs is critical for elucidating EV origins and
69 functions. The purification of EVs requires the recovery of apoplasts that are not
70 contaminated with the inner cellular components and vascular components. Obtaining
71 apoplasts from the imbibed leaf lumen via centrifugation is reportedly the optimal method
72 (Rutter et al., 2017). In this method, the apoplast recovery solution is infiltrated into the
73 leaf lumen and then gently recovered by a slow-speed centrifugation. The apoplasts are
74 subsequently collected following a density gradient centrifugation. The use of this method
75 resulted in the identification of 598 proteins in the EV fraction of Arabidopsis (Rutter and
76 Innes, 2017). Among these proteins, several EV markers, including tetraspanins and
77 SYP121, were identified, indicative of the successful recovery of EVs. Additionally,
78 biotic and abiotic stress-responsive proteins, membrane trafficking proteins, plasma
79 membrane-localized proteins, and vacuolar proteins were enriched. Moreover, several
80 ribosomal proteins, cytoplasmic enzymes, and cell wall-associated proteins were also
81 identified. Similarly, 237 proteins were identified in the EV fraction of sunflower
82 seedlings (Regente et al., 2017). The protein composition did not differ significantly from
83 that of the Arabidopsis EV fraction. The increase in EV secretion following an infection
84 by pathogenic fungi and bacteria may be associated with a change in the EV protein
85 composition (e.g., increase in the abundance of resistance-related proteins). However, a
86 previous study on Arabidopsis showed the EV contents are not significantly affected by
87 a *Pseudomonas syringae* infection (Rutter and Innes, 2017). An in depth analysis of the
88 EV proteome of *Botrytis cinerea*-infected Arabidopsis identified 981 proteins including

89 several RNA-binding proteins (e.g., AGO1 and the DEAD-box RNA helicases RH11 and
90 RH37) (He et al., 2021).
91
92 In this study, we conducted a proteomic analysis of Arabidopsis EVs obtained from
93 cell culture supernatants. The protein composition of the EV proteome was similar to that
94 of plasmodesmata (PD) proteomes (Fernandez-Calvino et al., 2011; Brault et al., 2019).
95 Confocal microscopy images revealed that a typical PD marker, PDLP3-GFP, was
96 localized to small particles in the apoplast region where PDs are absent. The optimized
97 iodixanol density gradient ultracentrifugation proteomic analysis and the in depth
98 clustering analysis enabled the separation of EV and PD proteins. The apoplast-secreted
99 EV- and PD-related proteins newly identified in this study will be useful for future
100 research on plant apoplasts as well as investigations involving EV and PD.
101
102

Results

Extracellular vesicles were detected in the plant cell culture medium

The supernatant of a plant cell culture is ideal biochemical materials for plant apoplast studies. More specifically, it is highly homogeneous and can be obtained from large cell cultures relatively easily. Thus, to study plant EVs, we focused on cell culture supernatants. First, to verify the presence of EVs in plant cell culture supernatants, the cell culture supernatant of tobacco BY-2 cells or Arabidopsis MM2d cells were prepared via centrifugation for the subsequent analysis (Fig. 1A). The sedimented fraction on the Percoll cushion was stained with BODIPY TR Ceramide to detect sphingolipids, which are abundant in animal EVs. Many particles were detected only in the sedimented fraction on the Percoll cushion (Fig. 1B, C and D, Supplemental Movie 1). To analyze these sedimented particles, the size and number of particles were measured using qNano. The results showed that the size of these particles ranged from 70 to130 nm with a peak at 87.5 nm (Fig. 1E). The size distribution of these particles is similar to that of typical exosome like EVs (Meldolesi 2018). Furthermore, to check whether EVs were collected in the sedimented fraction, we used green fluorescent protein (GFP)-tagged SYP121, which is a plant EV marker (He et al., 2021; Rutter and Innes, 2017). The SYP121-GFP signal was detected in the sedimented fraction on the Percoll cushion and overlapped with BODIPY TR Ceramide staining (Fig. 1F). These results indicated that EVs obtained from plant cell culture supernatants.

The Arabidopsis cell culture EVs proteome revealed the EV protein composition more accurately than the earlier seedling apoplast EV proteomes

To characterize the cell culture EVs, we collected EVs from the supernatant of a

127 healthy 7-day old MM2d cell culture (Supplemental Figure 1) and analyzed the protein
128 composition of the Arabidopsis MM2d EV fraction by mass spectrometry. A total of 1,356
129 proteins were identified in the cell culture EV proteome (Supplemental Table 1),
130 including 8.2% and 24.1% of the proteins in the seedling apoplast EV proteome identified
131 by He et al. (2021) and Rutter and Innes (2017), respectively (Fig. 2A). The major
132 proteins in the cell culture EV proteome were apoplast-related proteins, membrane
133 trafficking proteins, cell wall-associated proteins, plasma membrane proteins, membrane
134 transporters, and PD-related proteins (Fig. 2B).

135 Compared with the earlier analyses of seedling apoplast EV proteomes, our
136 examination of the cell culture EV proteome identified more proteins, including specific
137 protein subgroups predicted to have overlapping functions. This indicates that cell culture
138 EVs may provide a more comprehensive overview of the EV proteome than seedling
139 apoplast EVs. For example, of the 17 tetraspanin proteins in Arabidopsis (Cnops et al.,
140 2006), only one (TET8) was identified in the seedling apoplast EV proteome (Rutter and
141 Innes, 2017; He et al., 2021) (Fig. 2C). In contrast, eight of the 10 highly conserved plant
142 tetraspanins (TET1–TET10) were identified in the cell culture EVs (Fig. 2D). TET11–
143 TET17, which are less conserved tetraspanin family members (Fig. 2D) and lack
144 homologs in other plants (Cnops et al., 2006), were not identified. Accordingly, TET1–
145 TET10 are likely the functional tetraspanins in plant EVs.

146

147 Membrane trafficking proteins were also identified as EV proteins (Fig. 2E). For
148 example, SYP121 and its functional ortholog SYP122, were identified in both the cell
149 culture EV and seedling apoplast EV proteomes. In addition, VAMP721/VAMP722,
150 which participate in the fusion of MVBs to the plasma membrane together with

151 SYP121/SYP122 (Kwon et al., 2008), were also identified in both the cell culture EV and
152 seedling apoplast EV proteomes. Unlike seedling apoplast EV proteomes, the cell culture
153 EV proteome was enriched with specific subgroups of MVBs, such as ESCRT-0 and
154 ESCRT-3 complexes and the VPS4 complex, but not ESCRT-1 and ESCRT-2 (Fig. 2E).
155 Thus, compared with the previously characterized EV proteomes, the cell culture EV
156 proteome may provide additional insights into plant EV protein compositions.

157 In addition to the typical EV proteins, the cell culture EV proteome contained many
158 membrane trafficking proteins, including specific subgroups of small GTPases (ARF,
159 RAB, and ROP) (Supplemental Table 2). Earlier research showed ARA6/AtRABF1 helps
160 mediate the fusion of MVBs to plasma membranes (Ebine et al., 2012). Additionally,
161 AtRABA1a is colocalized with VAMP721/722 and facilitates the transport between the
162 TGN and the plasma membrane (Asaoka et al., 2013). Both AtRABD2a and AtRABD2b
163 are also involved in the transport from the TGN to the plasma membrane (Pinheiro et al.,
164 2009; Drakakaki et al., 2012). The SCAMP family members, which help transport
165 vesicles to the plasma membrane (Toyooka et al., 2009), were also enriched in the cell
166 culture EV proteome. There were some differences between the cell culture EV proteome
167 and the seedling apoplast EV proteome. More specifically, all clathrin heavy and light
168 chains and many clathrin-related proteins were detected in the seedling apoplast EV
169 proteome (He et al., 2021). Conversely, most of these proteins were not identified in the
170 cell culture EV proteome (Supplemental Table 2). Similarly, there were differences in the
171 identified EXOCYST-related components (Supplemental Table 2). The membrane
172 trafficking proteins detected in the cell culture EV proteome mediate various types of
173 transport to the plasma membrane, suggesting the cell culture EV fraction contained
174 various types of EVs.

175 Transporters, proton pumps, and auxin carriers, which are plasma membrane proteins,
176 were also detected in the cell culture EV proteome (Supplemental Table 3). These proteins
177 are ubiquitinated and transported to vacuoles for degradation via the MVB pathway
178 (Mosesso et al., 2019). If MVBs are transported to the plasma membrane rather than to
179 the vacuolar membrane, the vesicles within the MVBs are considered to be EVs.
180 Therefore, it is not surprising that these proteins were identified in EVs.

181 O-Glycosyl hydrolases that degrade β-1,3-glucan were relatively abundant in the cell
182 culture EV fraction. Among the 51 O-glycosyl hydrolase family 17 members in
183 Arabidopsis, 25 were previously predicted to contain the GPI-anchor motif that binds to
184 membranes (Doxey et al., 2007). In the cell culture EV proteome, 23 O-glycosyl
185 hydrolases were identified, of which 18 had the GPI-anchor motif, suggesting that
186 membrane-bound O-glycosyl hydrolases are selectively concentrated in the cell culture
187 EV proteome (Supplemental Table 4). Some O-glycosyl hydrolases were detected in
188 seedling apoplast EV proteomes, but they have not been thoroughly characterized.

189 The cell culture EV proteome also included several enzymes, such as strictosidine
190 synthase, eukaryotic aspartyl protease, purple acid phosphatase, and rotamase CYP,
191 which were previously identified in the apoplast proteome (Supplemental Table 1)
192 (Uemura et al., 2019). Although their exact functions are unknown, these enzymes might
193 modulate secondary metabolite metabolism or cell wall regulation in apoplasts.

194

195 ## The EV and PD proteomes had similar compositions

196 Rutter and Innes (2017) reported that the identified proteins in the seedling apoplast
197 EV proteome overlapped approximately 50% of the identified proteins in the PD
198 proteome (Fernandez-Calvino et al., 2011) and the membrane trafficking-related

199 proteome (Heard et al., 2015). In the current study, the identified proteins in the cell
200 culture EV proteome included many PD proteins. In terms of the top 30 high-intensity
201 proteins in the cell culture EV proteome, major plant EV markers, such as tetraspanins
202 (TET8 and TET1) and SNAREs (SYP121, SYP122, and SYP132), were identified in both
203 EV and PD proteomes (Fig. 3A) (Fernandez-Calvino et al., 2011; Brault et al., 2019).
204 Moreover, major PD markers, such as PDLP and PCBP family members, were also
205 identified in the cell culture EV proteome (Fig. 3A). Several specific proteins, including
206 the disease resistance-related protein NDR1, late embryogenesis abundant (LEA)
207 proteins, O-glycosyl hydrolases, and oxidases (including SKU5 family members) were
208 common to the EV and PD proteomes (Fig. 3A).

209 Of the 115 proteins identified in an earlier analysis of a PD proteome (Brault et al.,
210 2019), 77 were detected in the cell culture EV proteome (Fig. 3B). Among the 50 proteins
211 with the highest scores in the PD proteome (Brault et al., 2019), 43 were also identified
212 in the cell culture EVs. A similar correlation was also observed between the seedling
213 apoplast EV proteome (Rutter and Innes, 2017) and the PD proteome (Fernandez-Calvino
214 et al., 2011); 113 proteins in the PD proteome were also among the 204 proteins in the
215 seedling EV proteome (Fig. 3B). In the previous proteomic analyses, PDs were isolated
216 from the supernatant of cell wall-digested cultures by differential centrifugation. Isolated
217 PDs are reported as membranous components containing 50–100 nm vesicle-like
218 structures (Fernandez-Calvino et al., 2011). Hence, they are similar in size to EVs. Due
219 to the similarities in the purification protocols and vesicle sizes, it seems that the
220 separation of EVs from PDs was difficult.

221

222 PDLP3 localized to small particles in the apoplast and was distinguishable from

223 EVs

224 This study identified the amount of PD-related factors in the cultured cell supernatant
225 fraction (Fig 3). However, large membrane structures, as seen in the purified fraction in
226 the PD proteome analysis (Fernandez-Calvino et al., 2011), were not observed in the
227 cultured cell supernatant fraction. Therefore, we considered the possibility that PD-
228 related factors are secreted into the extracellular space as small particles.

229 To assess this possibility, we used an established PD marker line, pPDLP3::PDLP3-
230 GFP transgenic seedling (Thomas et al., 2008) and checked the localization by a spinning-
231 disc confocal laser microscopy equipped with hyper-sensitive sCMOS cameras (Fig. 4A).
232 PDLP3-GFP clearly localized to PDs (Fig. 4A). In addition, observations with a hyper-
233 sensitive camera showed that PDLP3-GFP localized to particles in cells such as
234 membrane trafficking vesicles (Fig. 4B) as previously reported (Thomas et al., 2008).
235 Observations with a hyper-sensitive camera also revealed that PDLP3-GFP particles
236 localized to both the plasma membrane and the extracellular region of hypocotyl
237 epidermal cells (Fig. 4C, D). Timelapse analyses revealed that signals of extracellular
238 PDLP3-GFP particles were immobile, sticking one spot for a long time (Fig. 4E,
239 Supplemental Movie 2), whereas signals of plasma membrane-bound PDLP3-GFP
240 particles showed intense two-dimensional motility (Fig. 4F, Supplemental Movie 2).
241 These results showed that PDLP3-GFP secreted into apoplastic regions where PDs are
242 absent.

243 Next, we checked whether the extracellular PDLP3-GFP particles were identical to
244 EVs. To assess this possibility, we selected TagRFP-SYP121 (Ebine et al. 2011) as an EV
245 marker. Observation of the sample mounting water of stable transgenic plants expressing
246 PDLP3-GFP and TagRFP-SYP121 showed that the particles of PDLP3-GFP and

247 TagRFP-SYP121 were independent (Fig. 4G), indicating that the extracellular PDLP3-
248 GFP particles are not identical to EVs.
249

250 The EV and PD proteins were distinguished by a density gradient 251 ultracentrifugation

252 The differences in the EV and PD protein localization implied these proteins may be
253 separated experimentally. To generate more pure EV fractions, we separated the crude EV
254 fractions by density gradient ultracentrifugation. The crude EV fractions were collected
255 from the cell culture supernatants by ultracentrifugation and then used for the 24%–3%
256 step-wise iodixanol density gradient ultracentrifugation, which resulted in six fractions
257 (Fig. 5A) that were subjected to the size distribution analysis and the proteome analyses.
258 Although the size distribution analysis did not show significant differences between
259 fractions (Supplemental Figure 2), the proteome analyses identified 524 proteins (Fig. 5B,
260 Supplemental Table 5).

261 The 524 identified proteins were classified into 18 clusters according to their
262 distribution (Fig. 5B, Supplemental Table 5). Tetraspanin and SNARE proteins were
263 distributed between 6% and 12% (fractions 2, 3, and 4), suggesting that typical EVs in
264 plant cell cultures are distributed between 6% and 12% (Fig. 6A). The PDLP (PDLP1, 3,
265 and 6) and PDCB (PDCB1 and 4) proteins, which are representative PD proteins, were
266 also distributed between 6% and 12% (fractions 2, 3, and 4) (Fig. 6B). The EV markers
267 were often most concentrated in fraction 4, followed by fractions 2 and then 3 or they
268 were exclusively concentrated in fraction 4 (Fig. 6A), whereas the PD markers were most
269 enriched in fraction 2, followed by fractions 3 and then 4 (Fig. 6B). Accordingly, although
270 it is likely difficult to completely separate EVs and PD, the EV markers can be

271 distinguished from the PD markers by iodixanol density gradient ultracentrifugation and
272 clustering analyses.

273 We subsequently classified additional proteins in the EV, PD, and Other categories.
274 Among the membrane trafficking markers, the SNAREs VAMP721, VAMP724, and
275 YKT61 as well as SYP121 and SYP122 were classified in the EV category (Fig. 6A).
276 Among the ESCRT proteins involved in MVB formation, CHMP2A and VPS24A were
277 classified in the EV category, whereas CHMP2B, VPS20B, and SNF7A were classified
278 in the PD category (Fig. 6C). Moreover, SCAMP and the RAB GTPases were also divided
279 into the EV and PD categories (Fig. 6C). The crude EV fraction contained many
280 transporters belonging to the PD, EV, and Other categories (Fig. 6D). In the Other
281 category, NRT1:2, proton transporters, and auxin transporters were concentrated in the
282 heaviest fraction (i.e., fraction 6). The NDR1/HIN1 family, which is involved in disease
283 resistance, was clearly concentrated in the EV category (Fig. 6E). The LEA family, which
284 is phylogenetically closely related to the NDR1/HIN1 family, was classified in either the
285 EV or PD category (Supplemental Table 5). In addition, the PTI1 family, which comprises
286 key signaling proteins related to disease resistance (Sun et al., 2022), was concentrated in
287 the EV category (Fig. 6E).

288 A number of transporters were classified in the PD category, among which CHER1
289 (choline transporter) is localized in TGNs, cell plates, and sieve pores after cell division;
290 it is important for the development of sieve pores and PD (Dettmer et al., 2014; Kraner
291 et al., 2017; Gao et al., 2017b). Although CHER1 has not been confirmed as a PD-
292 localized protein, it was classified in the PD category in this study. Other transporters in
293 the PD category may also affect PD development and functions.

294 Oxidases and peroxidases, which regulate the apoplast redox state and pH homeostasis,

295 were relatively abundant in the crude EV fraction. The apoplast redox state and pH
296 homeostasis are crucial factors influencing cell expansion, development, and defenses
297 against pathogens (Smirnoff and Arnaud, 2019). Both SKU5 and SKS1 contribute to cell
298 wall formation (Chen et al., 2023; Sedbrook et al., 2002). In the present study, SKS3 and
299 SKS1 were classified in the PD and EV categories, respectively (Fig. 6F). Furthermore,
300 SKU5, SKS5, and SKS12 were concentrated in fractions 4 and 5, which were slightly
301 heavier than the EV fraction. Interestingly, most of the other oxidases and peroxidases
302 were also concentrated in fractions 4 and 5. Beta-glucosidases were also enriched in
303 fractions 4 and 5, one of which (BGLU15) is an apoplastic enzyme that mediates the
304 degradation of flavonol bisglycosides (Roepke et al., 2017). These results suggest that
305 oxidases, peroxidases, and beta-glucosidases are localized to some apoplastic structures
306 other than EVs and PD.

307 The beta-1,3-glucanases, which are O-glycosyl hydrolases involved in degrading
308 callose, were widely distributed in each fraction. Earlier research showed PdBG1, PdBG2,
309 and PdBG3 are localized to PD (Levy et al., 2007; Benitez-Alfonso et al., 2013). In the
310 current study, PdBG2 was classified in the PD category, but PdBG1 and PdBG3 were
311 concentrated in the lightest fraction (i.e., fraction 1) (Fig. 6G). Moreover, BG_pap is a
312 PD-localized beta-1,3-glucanase (Levy et al., 2007; Zavaliev et al., 2016). However,
313 BG_pap was abundant in the heaviest fraction (i.e., fraction 6) (Fig. 6G). The EV fractions
314 contained ZERZAUST, which is an important O-glycosyl hydrolase for intercellular
315 communication (Vaddepalli et al., 2017). In addition, several O-glycosyl hydrolases were
316 enriched in the EV fraction (Fig. 6G). These findings suggest that O-glycosyl hydrolases
317 are localized to various structures in the apoplast.
318

319 **Discussion**

320 Extracellular vesicles are membrane-coated vesicles in apoplasts. These vesicles are
321 transported via various membrane trafficking pathways and degradation pathways.
322 Plasmodesmata connect neighboring cells as cell wall-embedded structures consisting of
323 the plasma membrane, cytoplasm, and ER. The apoplast side of PD accumulates callose
324 and some specific components, including callose-binding proteins, callose synthases, and
325 callose degrading enzymes (β-1,3-glucanases). On the basis of these distinct structural
326 differences, EVs and PD are generally considered to be different structures.

327 The EV proteomes analyzed in a previous study (Rutter and Innes, 2017) and in the
328 current study were revealed to contain a considerable abundance of PD proteins. Similarly,
329 earlier examinations of PD proteomes identified EV proteins (Fernandez-Calvino et al.,
330 2011; Brault et al., 2019). Hence, EV and PD proteins were not separated in previous
331 proteome-level investigations, possibly because of the similarities in the purification
332 methods. More specifically, EVs were purified from the apoplast fraction by
333 centrifugation, while PD were purified via the centrifugation of solutions comprising
334 digested cell walls. The reported size of EVs (50–300 nm) (Rutter and Innes, 2017) is
335 similar to the size of vesicle-like PD structures purified from the cellulase-digested cell
336 wall fraction (50–100 nm) (Fernandez-Calvino et al., 2011).

337 In the present study, we distinguished EVs from PD on the basis of a density gradient
338 centrifugation and fine-tuned clustering. We revealed the differences in the clustering of
339 typical EV markers, such as tetraspanins and specific SNARE family members, and
340 typical PD markers, such as PDLP and PDCB proteins. Recent analyses of the
341 *Physcomitrium patens* PD proteome successfully identified core PD proteins (Johnston
342 et al., 2023; Gombos et al., 2023). The PDLP and PDCB families are apparently not

343 conserved in *P. patens* or in *Marchantia polymorpha* and *Klebsormidium nitens* (Bowman
344 et al., 2017), implying that the fraction containing the PDLP and PDCB proteins in this
345 study may not be the PD fraction that includes the desmotubule. A number of unclassified
346 clusters were identified in this study (Figure 5 and Supplemental Table 5). Of these,
347 cluster 18, which was enriched in the heaviest fraction (i.e., fraction 6), is notable because
348 it contained MCTP4, but lacked typical PD markers. The MCTP4 protein belongs to the
349 MCTP family, which may be involved in linking the ER membrane and the plasma
350 membrane within PD (Brault et al., 2019). Additionally, among the SNARE proteins, only
351 SYP71 was classified in cluster 18. This protein is localized to the plasma membrane, ER,
352 and cell plate (Suwastika et al., 2008; El Kasmi et al., 2013). These results suggest that
353 cluster 18 may be enriched with proteins linking the desmotubule to the plasma
354 membrane in PD. In the current study, the PD fraction including the PDLP and PDCB
355 proteins was slightly lighter than the EV fraction, suggesting that the PD fraction may
356 consist of only small particles (e.g., vesicles) and proteins that aggregate on the apoplast
357 side of PD. The heavy fraction (i.e., cluster 18) may contain PD. Clarifying whether the
358 proteins in cluster 18 actually belong to desmotubule–plasma membrane structures in PD
359 may require additional electron microscopy analyses.
360
361 In contrast to plant seedlings, cultured cells are undifferentiated and homogeneous. In
362 this study, we originally planned to recover pure homogeneous EVs via the
363 ultracentrifugation of a large volume of cell culture supernatant. However, the recovered
364 fraction contained various apoplast granules, including PD-associated proteins and
365 apoplast proteins as well as EV proteins. The density gradient centrifugation and
366 clustering categorized these proteins into 18 clusters, but it is unclear whether apoplast

granules and structures remained. The study findings indicate that the secretion of apoplast materials is a complex process, even in homogeneous cell cultures. Plant seedlings consisting of various differentiated cells secrete more complex apoplast components. Furthermore, the types and amount of secreted apoplast components are influenced by biotic and abiotic stimuli. Future analyses of the clusters identified in this study will further characterize apoplast structures and physiological responses in plant seedlings.

375 **Materials and Methods**

376 Growth conditions of Arabidopsis cultured cells

377 Arabidopsis MM2d cells (Menges and Murray, 2002) and tobacco BY-2 cells were
378 cultured in modified LS medium (Nagata et al., 1981) on a rotary shaker (130 rpm) at
379 27 °C in darkness. To maintain the cell culture, 3 mL 7-day-old MM2d cultured cells were
380 transferred to 95 mL fresh medium in 300 mL flasks. Arabidopsis plants (Col-0) were
381 grown on 1.5% agar medium containing 1% sucrose and 1% MES-KOH (pH 5.7) in plates
382 and in half-strength Murashige and Skoog salt medium at 22 °C for 5 days.

383

384 Isolation of EVs from the culture medium

385 Seven-day-old MM2d cell cultures were centrifuged twice (1,500 × g for 5 min). The
386 supernatants were collected for the high-speed centrifugation (10,000 × g for 1 h), which
387 was completed to eliminate any remaining debris. The purified cell culture supernatants
388 were placed on a Percoll cushion (37% Percoll and 0.6 M sorbitol) prepared in a
389 centrifuge tube for the subsequent ultracentrifugation (100,000 × g for 1 h). The white
390 layer on the Percoll cushion was recovered. The EVs were further purified using exoEasy
391 Maxi kit (Qiagen). The resulting samples, which were designated as EV fractions, were
392 used for the mass spectrometry analysis.

393 For the density gradient ultracentrifugation, the supernatants of 5-day-old MM2d cell
394 cultures were prepared via the centrifugations described above and collected from the top
395 of the 24% iodixanol solution containing 0.25 M sucrose and 20 mM HEPES-KOH (pH
396 7.4) after the ultracentrifugation (100,000 × g for 1 h). The collected crude EV fractions
397 were diluted with 10 volumes of buffer (0.25 M sucrose and 20 mM HEPES-KOH, pH
398 7.4) before the density gradient ultracentrifugation (100,000 × g for 1 h) involving the

399 24%, 12%, 6%, and 3% step-wise iodixanol density gradient. Each layer was recovered
400 and used for the mass spectrometry analysis.
401

402 ## Size distribution and particle concentration

403 The size and number of particles in each fraction were analyzed using qNano (Izon,
404 Christchurch, New Zealand). The NP200 nanopore and CPC100 calibration sample were
405 used for particle detection and evaluation.
406

407 ## Mass spectrometry

408 The mass spectrometry analysis was performed as described by Imami et al. (2018),
409 with slight modifications. Proteins were precipitated in 20% trichloroacetic acid (TFA).
410 The pelleted proteins were washed three times in ice-cold 100% acetone and then
411 resuspended in 50 μL resuspension buffer (8 M urea and 0.1 M Tris-HCl, pH 8). After
412 adding 10 mM dithiothreitol, the proteins were reduced at room temperature for 30 min
413 and then alkylated using 50 mM iodoacetamide at room temperature for 30 min in
414 darkness. Proteins were digested with lysyl endopeptidase (LysC) (Wako) at room
415 temperature for 3 h. The sample solutions were diluted to a final concentration of 2 M
416 urea and 50 mM ammonium bicarbonate prior to the trypsin (Promega) digestion, which
417 was performed with constant agitation at room temperature for 16 h. The resulting peptide
418 samples were desalted using SDB-XC (upper)/SCX (bottom) (GL Sciences) StageTips
419 (Adachi et al., 2016). The peptides were sequentially eluted using elution buffer 1 (4%
420 TFA, 500 mM ammonium acetate, and 30% acetonitrile) and elution buffer 2 (500 mM
421 ammonium acetate and 30% acetonitrile).
422 The nano-scale reversed-phase liquid chromatography and tandem mass spectrometry

423 (nanoLC/MS/MS) analysis was completed using the Orbitrap Fusion Lumos mass
424 spectrometer (Thermo Fisher Scientific) connected to a Thermo Ultimate 3000
425 RSLCnano pump and an HTC-PAL autosampler (CTC Analytics, Zwingen, Switzerland)
426 equipped with a self-packing analytical column (150 mm long with 100 μm internal
427 diameter) (Ishihama et al., 2002) packed with ReproSil-Pur C18-AQ (3 μm; Dr. Maisch
428 GmbH). Mobile phase A consisted of 0.5% acetic acid, whereas mobile phase B
429 comprised 0.5% acetic acid and 80% acetonitrile. Peptides were eluted from the analytical
430 column at a flow rate of 500 nL/min with the following gradient: 5%–10% B in 5 min,
431 10%–40% B in 20 min, 40%–99% B in 1 min, and 99% for 5 min. The Orbitrap Fusion
432 Lumos instrument was operated in the data-dependent mode with a full scan in the
433 Orbitrap followed by MS/MS scans for 3 s for the higher-energy collisional dissociation
434 (HCD). The applied voltage for ionization was 2.4 kV. The full scans were performed
435 with a resolution of 120,000, a target value of 4×10^5 ions, and a maximum injection time
436 of 50 ms. The MS scan range was m/z 300–1,500. The MS/MS scans were performed
437 with a resolution of 15,000, a target value of 5×10^4 ions, and a maximum injection time
438 of 50 ms. The isolation window was set to 1.6. The normalized HCD collision energy was
439 30. Dynamic exclusion was applied for 20 s.

440 All raw data files were analyzed and processed using MaxQuant (v1.6.15.0) (Cox and
441 Mann, 2008). Andromeda (Cox et al., 2011) was used to search the
442 Araport11_genes.201606.pep (https://www.arabidopsis.org/) database spiked with
443 common contaminants and enzyme sequences. The search parameters included two
444 missed cleavage sites and variable modifications, including methionine oxidation,
445 deamidation of glutamine and asparagine and protein N-terminal acetylation. Cysteine
446 carbamidomethylation was set as a fixed modification. The peptide mass tolerance was

447 4.5 ppm, whereas the MS/MS tolerance was 20 ppm. The false discovery rate at the
448 peptide spectrum match and protein levels was set to 1%.
449
450 Microscopy analyses
451 The confocal microscopy analysis was performed using the ECLIPSE Ti microscope
452 (Nikon) equipped with a confocal spinning disc unit (CSU-W1, Yokogawa) and the
453 sCMOS camera (Sona, Andor). The isolated EVs were stained with 1 μM BODIPY TR
454 Ceramide (ThermoFisher Scientific). For the optical sectioning of Arabidopsis seedlings,
455 transgenic plants expressing both PDLP3-GFP and TagRFP-SYP121 were mounted
456 between 60 × 24 and 18 × 18 coverslips (Iwanami) with a 0.15 mm spacer. Images were
457 captured using NIS-Element AR (Nikon) and analyzed using Fiji (Schindelin et al., 2012).
458
459
460 **Acknowledgements and fundings**
461 We thank Tsuyoshi Nakagawa (Shimane University) for providing Gateway binary
462 vectors containing bar gene identified by Meiji Seika Kaisha, Ltd., Andrew J. Maule
463 (John Innes Centre) for providing the PDLP3-GFP transgenic plant, Masa H. Sato and
464 Tomoko Hirano (Kyoto Pref. Univ.) for providing the pGWB1-GFP-SYP121 plasmid,
465 Kazuo Ebine and Takashi Ueda (NIBB) for providing the TagRFP-SYP121 seedling,
466 Akihiko Nakano (Riken) and Tomohiro Uemura (Ochanimizu Univ) for helpful
467 discussion. This study was supported by JST-PRESTO [JPMJPR18H7 to T. H.,
468 JPMJPR19H7 to K. Sueyoshi, and JPMJPR18H2 to K. I.] and JST-CREST
469 [JPMJCR18H4 to T. H. and JPMJCR19H1 to K. Sueyoshi].
470

471 **Figure legends**

472 Figure 1. Isolation of EVs from a plant cell culture suspension

473 **A)** Protocol for the isolation of EVs from plant cell cultures. **B–D)** BODIPY TR Ceramide
474 staining of the ultracentrifugation-derived sedimented fraction (B) and supernatant
475 fraction (C) for the tobacco BY-2 culture medium and the ultracentrifugation-derived
476 sedimented fraction for the medium before culturing (D). The panels on the right present
477 the enlarged images of the area marked by a white square in the panels on the left. These
478 images correspond to the optical section presented in Supplemental Movie 1. Bar, 2 μm.
479 **E)** Size distribution of sedimented particles by ultracentrifugation from the supernatant
480 of Arabidopsis MM2d cells. **F)** Purified EVs from SYP121-GFP transgenic tobacco BY-
481 2 cell cultures. Bar, 2 μm.

482

483 Figure 2. Comparison between the cell culture EV proteome and the seedling
484 apoplast EV proteome

485 **A)** Venn diagram of the identified proteins in the cell culture EV proteome and the
486 seedling apoplast EV proteome. **B)** Classification of the top 100 high-intensity proteins
487 in the cell culture EV proteome. **C)** Identified tetraspanin family members in the cell
488 culture EV proteome and the seedling apoplast EV proteome. **D)** Phylogenetic tree of the
489 tetraspanin family in *Arabidopsis thaliana*. Identified tetraspanin family members in the
490 cell culture EV proteome were colored in gray. **E)** Identified membrane trafficking
491 proteins in the cell culture EV proteome and the seedling apoplast EV proteome.

492

493 Figure 3. Comparison between the EV proteome and the plasmodesmata
494 proteome

495 **A)** Comparison of the EV proteomes and the plasmodesmata proteomes in terms of the
496 top 30 high-intensity proteins in the cell culture EV proteomes. **B)** Overlap percentages
497 between the three EV proteomes and the two plasmodesmata proteomes. The EV and
498 plasmodesmata fractions were indistinguishable in these analyses.
499

500 Figure 4. Localization of PDLP3-GFP in the apoplast region

501 **A-D)** Confocal microscopy images of PDLP3-GFP. Plasma membrane was labeled by
502 Plasmembrane Red. PDLP3-GFP clearly localized to plasmodesmata (A, white
503 arrowheads). At high contrast images, the PDLP3-GFP signals were also observed as
504 particles at inside (B), plasma membrane (C), and surface (D). Some PDLP3-GFP signals
505 were detected as small particles in the apoplast region (D, white arrowheads). Bar, 10 μm.
506 **E, F)** Projection images from PDLP3-GFP time-lapse analyses. The 15 time-lapse images
507 were acquired every 5 seconds and grouped into early (1-5), middle (6-10), and late (11-
508 15) phases. These images were projected at maximum intensity, and superimposed into
509 one merge image using blue, green and red colour, respectively. Bars, 10 μm. **G)**
510 Comparison of PDLP3-GFP and TagRFP-SYP121 at the apoplast region. TagRFP-
511 SYP121 (white arrowheads) were not colocalized with PDLP3-GFP (yellow arrowheads).
512 Bar, 5 μm.
513

514 Figure 5. Iodixanol density gradient ultracentrifugation of the crude EV fraction

515 A) Separation of the crude EV fraction by an iodixanol density gradient
516 ultracentrifugation. The crude EV fraction was mounted on the top of the iodixanol
517 solution during the density gradient ultracentrifugation (24%, 12%, 6%, and 3% iodixanol
518 solutions). After the ultracentrifugation, six fractions were recovered and used for

519 proteome analyses. B) Classification of the 524 identified proteins on the basis of their
520 distribution. The presented data correspond to the information provided in Supplemental
521 Table 5.
522
523 Figure 6. Representative proteins in each gene ontology category
524 A) Representative EV proteins. **B)** Representative PD proteins. **C)** Membrane trafficking-
525 related proteins. **D)** Membrane transporters and pumps. **E)** Disease resistance-related
526 proteins. **F)** Oxidases and peroxidases. **G)** O-glycosyl hydrolases. The presented data
527 correspond to the information provided in Supplemental Table 5. cl. indicates the cluster
528 number in Figure 5B; cat. indicates category.
529
530
531 Supplemental Figure 1. Growth condition of MM2d Arabidopsis cultured cells for
532 this study
533 **A)** Growth curve of MM2d Arabidopsis cultured cells in this study. Supernatant of 5 days-
534 old and 7 days-old cultured cells was applied for EV purification. **B)** DNA degradation
535 assay of MM2d cells. In 5 days-old and 7 days-old cultured cells, DNA degradation did
536 not occur at all.
537
538 Supplemental Figure 2. Size distribution of EVs in each fraction after an iodixanol
539 density gradient ultracentrifugation
540 Six fractions were recovered after an iodixanol density gradient ultracentrifugation and
541 used for size distribution analyses. These fractions correspond to the fractions in Figure
542 5A.

543

544 Supplemental Table 1 List of 1356 proteins identified in the cultured cell EV
545 proteomics

546

547 Supplemental Table 2 Comparison of membrane traffic proteins between the cultured
548 cell and the leaf apolast EV proteomics

549

550 Supplemental Table 3 Comparison of transpoters and ubiquitin-related proteins
551 between the cultured cell and the leaf apolast EV proteomics

552

553 Supplemental Table 4 Comparison of O-Glycosyl hydrolases family 17 proteins
554 between the cultured cell and the leaf apolast EV proteomics

555

556 Supplemental Table 5 List of 524 proteins Identified in the density gradient ultra-
557 centrifugation proteome

558

559 Supplemental Movie 1 Optical sections of isolated EVs.
560 EVs were stained by BODIPY TR Ceramide. Images were taken from the surface of
561 coverslip toward to the top of a drop.

562

563 Supplemental Movie 2 Time-lapse analyses of PDLP3-GFP.
564 Images were taken from the same seedling at different depths. These images were used
565 to generate the projection images of Figure 4E and F. Bars, 10 μm.

566

567 **References**

568

569 **Adachi, J., Hashiguchi, K., Nagano, M., Sato, M., Sato, A., Fukamizu, K.,**
570 **Ishihama, Y., and Tomonaga, T.**. Improved proteome and phosphoproteome
571 analysis on a cation exchanger by a combined acid and salt gradient. Anal. Chem.
572 2016:**88**: 7899–7903.

573 **Asaoka, R., Uemura, T., Ito, J., Fujimoto, M., Ito, E., Ueda, T., and Nakano, A.**.
574 Arabidopsis RABA1 GTPases are involved in transport between the trans-Golgi
575 network and the plasma membrane, and are required for salinity stress tolerance.
576 Plant J. 2013:**73**: 240–249.

577 **Assaad, F.F., Qiu, J.-L., Youngs, H., David, E., Zimmerli, L., Kalde, M., Wanner,**
578 **G., Peck, S.C., Edwards, H., Ramonell, K., Somerville, C.R., and Thordal-**
579 **Christensen, H.** The PEN1 Syntaxin Defines a Novel Cellular Compartment upon
580 Fungal Attack and Is Required for the Timely Assembly of Papillae. Mol Biol Cell
581 2004:**15**: 5318–5328.

582 **Benitez-Alfonso, Y., Faulkner, C., Pendle, A., Miyashima, S., Helariutta, Y., and**
583 **Maule, A.** Symplastic Intercellular Connectivity Regulates Lateral Root
584 Patterning. Dev. Cell 2013:**26**: 136–147.

585 **Bowman, J.L. et al.** Insights into Land Plant Evolution Garnered from the Marchantia
586 polymorpha Genome. Cell 2017:**171**: 287-304.e15.

587 **Brault, M.L. et al.** Multiple C2 domains and transmembrane region proteins (MCTP s)
588 tether membranes at plasmodesmata . EMBO Rep. 2019:**20**: 1–26.

589 **Chen, C. et al.** Multi-copper oxidases SKU5 and SKS1 coordinate cell wall formation
590 using apoplastic redox-based reactions in roots. Plant Physiol. 2013:**192**: 2243–
591 2260.

592 **Clough, S.J. and Bent, A.F.** Floral dip: A simplified method for Agrobacterium-
593 mediated transformation of Arabidopsis thaliana. Plant J. 1998:**16**: 735–743.
594 **Cnops, G. et al.** The TORNADO1 and TORNADO2 genes function in several
595 patterning processes during early leaf development in Arabidopsis thaliana. Plant
596 Cell 2006:**18**: 852–866.
597 **Collins, N.C., Thordal-christensen, H., and Lipka, V.** SNARE-protein-mediated
598 disease resistance at the plant cell wall. Nature 2003:**312**: 310–312.
599 **Cox, J. and Mann, M.** MaxQuant enables high peptide identification rates,
600 individualized p.p.b.-range mass accuracies and proteome-wide protein
601 quantification. Nat. Biotechnol. 2008:**26**: 1367–1372.
602 **Cox, J., Neuhauser, N., Michalski, A., Scheltema, R.A., Olsen, J. V, and Mann, M.**
603 Andromeda : A Peptide Search Engine Integrated into the MaxQuant
604 Environment.: 2011:**10(4)**:1794–1805.
605 **Cui, Y., Gao, J., He, Y., and Jiang, L.** Plant extracellular vesicles. Protoplasma
606 2020:**257**: 3–12.
607 **Dettmer, J. et al.** CHOLINE TRANSPORTER-LIKE1 is required for sieve plate
608 development to mediate long-distance cell-to-cell communication. Nat. Commun.
609 2014:**4276**.
610 **Doxey, A.C., Yaish, M.W.F., Moffatt, B.A., Griffith, M., and McConkey, B.J.**
611 Functional divergence in the Arabidopsis β-1,3-glucanase gene family inferred by
612 phylogenetic reconstruction of expression states. Mol. Biol. Evol. 2007:**24**: 1045–
613 1055.
614 **Drakakaki, G., Van De Ven, W., Pan, S., Miao, Y., Wang, J., Keinath, N.F.,**
615 **Weatherly, B., Jiang, L., Schumacher, K., Hicks, G., and Raikhel, N.** Isolation

616 and proteomic analysis of the SYP61 compartment reveal its role in exocytic
617 trafficking in Arabidopsis. Cell Res. 2012:**22**: 413–424.
618 **Ebine, K., Miyakawa, N., Fujimoto, M., Uemura, T., Nakano, A., and Ueda, T.**
619 Endosomal trafficking pathway regulated by ARA6, a RAB5 GTPase unique to plants.
620 Small GTPases 2012:**3**: 23–27.
621 **Fernandez-Calvino, L., Faulkner, C., Walshaw, J., Saalbach, G., Bayer, E.,**
622 **Benitez-Alfonso, Y., and Maule, A.** Arabidopsis plasmodesmal proteome. PLoS
623 One 2011:**6**.
624 **Gao, C., Zhuang, X., Shen, J., and Jiang, L.** Plant ESCRT Complexes: Moving
625 Beyond Endosomal Sorting. Trends Plant Sci. 2017a:**22**: 986–998.
626 **Gao, Y.Q., Chen, J.G., Chen, Z.R., An, D., Lv, Q.Y., Han, M.L., Wang, Y.L., Salt,**
627 **D.E., and Chao, D.Y.** A new vesicle trafficking regulator CTL1 plays a crucial
628 role in ion homeostasis. PLoS Biol. 2017b:**15**: 1–27.
629 **Gombos, S. et al.** A high-confidence Physcomitrium patens plasmodesmata proteome
630 by iterative scoring and validation reveals diversification of cell wall proteins
631 during evolution. New Phytol. 2023:**238**: 637–653.
632 **Hansen, L.L. and Nielsen, M.E.** Plant exosomes: Using an unconventional exit to
633 prevent pathogen entry? J. Exp. Bot. 2017:**69**: 59–68.
634 **He, B., Cai, Q., Qiao, L., Huang, C.Y., Wang, S., Miao, W., Ha, T., Wang, Y., and**
635 **Jin, H.** RNA-binding proteins contribute to small RNA loading in plant
636 extracellular vesicles. Nat. Plants 2021:**7**: 342–352.
637 **Heard, W., Sklenář, J., Tomé, D.F.A., Robatzek, S., and Jones, A.M.E.**
638 Identification of regulatory and cargo proteins of endosomal and secretory
639 pathways in arabidopsis thaliana by proteomic dissection. Mol. Cell. Proteomics

640 2015:**14**: 1796–1813.

641 **Imami, K., Milek, M., Bogdanow, B., Yasuda, T., Kastelic, N., Zauber, H.,**
642 **Ishihama, Y., Landthaler, M., and Selbach, M.** Phosphorylation of the
643 Ribosomal Protein RPL12/uL11 Affects Translation during Mitosis. Mol. Cell
644 2018:**72**: 84-98.e9.

645 **Ishihama, Y., Rappsilber, J., Andersen, J.S., and Mann, M.** Microcolumns with self-
646 assembled particle frits for proteomics. J. Chromatogr. A 2002:**979**: 233–239.

647 **Ito, Y. and Uemura, T.** Super resolution live imaging: The key for unveiling the true
648 dynamics of membrane traffic around the Golgi apparatus in plant cells. Front.
649 Plant Sci. 2022:**13**: 1–8.

650 **Johnston, M.G., Breakspear, A., Samwald, S., Zhang, D., Papp, D., Faulkner, C.,**
651 **and de Keijzer, J.** Comparative phyloproteomics identifies conserved
652 plasmodesmal proteins. J. Exp. Bot. 2023:**74**: 1821–1835.

653 **El Kasmi, F., Krause, C., Hiller, U., Stierhof, Y.D., Mayer, U., Conner, L., Kong,**
654 **L., Reichardt, I., Sanderfoot, A.A., and Jürgens, G.** SNARE complexes of
655 different composition jointly mediate membrane fusion in Arabidopsis cytokinesis.
656 Mol. Biol. Cell 2013:**24**: 1593–1601.

657 **Kraner, M.E., Link, K., Melzer, M., Ekici, A.B., Uebe, S., Tarazona, P., Feussner,**
658 **I., Hofmann, J., and Sonnewald, U.** Choline transporter-like1 (CHER1) is crucial
659 for plasmodesmata maturation in Arabidopsis thaliana. Plant J. 2017:**89**: 394–406.

660 **Kwon, C. et al.** Co-option of a default secretory pathway for plant immune responses.
661 Nature 2008:**451**: 835–840.

662 **Lee, J.Y., Wang, X., Cui, W., Sager, R., Modla, S., Czymmek, K., Zybaliov, B.,**
663 **Van Wijk, K., Zhang, C., Lu, H., and Lakshmanana, V.** A plasmodesmata-

664 localized protein mediates crosstalk between cell-to-cell communication and innate
665 immunity in arabidopsis. Plant Cell 2011:**23**: 3353–3373.
666 **Levy, A., Erlanger, M., Rosenthal, M., and Epel, B.L.** A plasmodesmata-associated
667 β-1,3-glucanase in Arabidopsis. Plant J. 2007:**49**: 669–682.
668 **Lipka, V. et al.** Plant science: Pre- and postinvasion defenses both contribute to
669 nonhost resistance in Arabidopsis. Science. 2005:**310**: 1180–1183.
670 **Matsui, H., Matsui, H., Fujiwara, M., Hamada, S., Shimamoto, K., Nomura, Y.,**
671 **Nakagami, H., Takahashi, A., and Hirochika, H.** Plasma membrane localization
672 is essential for oryza sativa pto-interacting protein 1a-mediated negative regulation
673 of immune signaling in rice. Plant Physiol. 2014:**166**: 327–336.
674 **Menges, M. and Murray, J.A.H.** Synchronous Arabidopsis suspension cultures for
675 analysis of cell-cycle gene activity. Plant J. 2002:**30**: 203–212.
676 **Meyer, D., Pajonk, S., Micali, C., O'Connell, R., and Schulze-Lefert, P.**
677 Extracellular transport and integration of plant secretory proteins into pathogen-
678 induced cell wall compartments. Plant J. 2009:**57**: 986–999.
679 **Meldolesi, J.** Exosomes and ectosomes in intercellular communication. Curr. Biol.
680 2018:28: R435-R444.
681 **Mosesso, N., Nagel, M.K., and Isono, E.** Ubiquitin recognition in endocytic trafficking
682 - With or without ESCRT-0. J. Cell Sci. 2019:**132**.
683 **Nagata, T., Okada, K., Takebe, I., and Matsui, C.** Delivery of tobacco mosaic virus
684 RNA into plant protoplasts mediated by reverse-phase evaporation vesicles
685 (Liposomes). MGG Mol. Gen. Genet. 1981:**184**: 161–165.
686 **Nakamura, S., Mano, S., Tanaka, Y., Ohnishi, M., Nakamori, C., Araki, M., Niwa,**
687 **T., Nishimura, M., Kaminaka, H., Nakagawa, T., Sato, Y., and Ishiguro, S.**

688 Gateway binary vectors with the bialaphos resistance gene, bar, as a selection
689 marker for plant transformation. Biosci. Biotechnol. Biochem. 2010:**74**: 1315–
690 1319.
691 **Nielsen, M.E. and Thordal-Christensen, H.** Recycling of Arabidopsis plasma
692 membrane PEN1 syntaxin. Plant Signal. Behav. 2012:**7**: 1541–1543.
693 **Otegui, M.S.** ESCRT-mediated sorting and intralumenal vesicle concatenation in
694 plants. Biochem. Soc. Trans. 2018:**46**: 537–545.
695 **Pinheiro, H., Samalova, M., Geidner, N., Chory, J., Martinez, A., and Moore, I.**
696 Genetic evidence that the higher plant Rab-D1 and Rab-D2 GTPases exhibit
697 distinct but overlapping interactions in the early secretory pathway. J. Cell Sci.
698 2009:**122**: 3749–3758.
699 **Regente, M., Pinedo, M., Clemente, H.S., Balliau, T., Jamet, E., and De La Canal,**
700 **L.** Plant extracellular vesicles are incorporated by a fungal pathogen and inhibit its
701 growth. J. Exp. Bot. 2017:**68**: 5485–5495.
702 **Roepke, J., Gordon, H.O.W., Neil, K.J.A., Gidda, S., Mullen, R.T., Freixas Coutin,**
703 **J.A., Bray-Stone, D., and Bozzo, G.G.** An apoplastic β-glucosidase is essential
704 for the degradation of flavonol 3-O-β-Glucoside-7-O-α-rhamnosides in
705 arabidopsis. Plant Cell Physiol. 2017:**58**: 1030–1047.
706 **Rutter, B., Rutter, K., and Innes, R.** Isolation and Quantification of Plant
707 Extracellular Vesicles. Bio-Protocol 2017:**7**: 1–13.
708 **Rutter, B.D. and Innes, R.W.** Extracellular vesicles isolated from the leaf apoplast
709 carry stress-response proteins. Plant Physiol. 2017:**173**: 728–741.
710 **Schindelin, J. et al.** Fiji: An open-source platform for biological-image analysis. Nat.
711 Methods 2012:**9**: 676–682.

712 **Sedbrook, J.C., Carroll, K.L., Hung, K.F., Masson, P.H., and Somerville, C.R.** The
713 Arabidopsis SKU5 gene encodes an extracellular glycosyl phosphatidylinositol-
714 anchored glycoprotein involved in directional root growth. Plant Cell 2002:**14**:
715 1635–1648.
716 **Smirnoff, N. and Arnaud, D.** Hydrogen peroxide metabolism and functions in plants.
717 New Phytol. 2019:**221**: 1197–1214.
718 **Sun, M., Qiu, L., Liu, Y., Zhang, H., Zhang, Y., Qin, Y., Mao, Y., Zhou, M., Du, X.,**
719 **Qin, Z., and Dai, S.** Pto Interaction Proteins: Critical Regulators in Plant
720 Development and Stress Response. Front. Plant Sci. 2022:**13**: 1–11.
721 **Suwastika, I.N., Uemura, T., Shiina, T., Sato, M.H., and Takeyasu, K.** SYP71, a
722 plant-specific Qc-SNARE protein, reveals dual localization to the plasma
723 membrane and the endoplasmic reticulum in Arabidopsis. Cell Struct. Funct.
724 2008:**33**: 185–192.
725 **Thomas, C.L., Bayer, E.M., Ritzenthaler, C., Fernandez-Calvino, L., and Maule,**
726 **A.J.** Specific targeting of a plasmodesmal protein affecting cell-to-cell
727 communication. PLoS Biol. 2008:**6**: 0180–0190.
728 **Toyooka, K., Goto, Y., Asatsuma, S., Koizumi, M., Mitsui, T., and Matsuoka, K.** A
729 mobile secretory vesicle cluster involved in mass transport from the golgi to the
730 plant cell exterior. Plant Cell 2009:**21**: 1212–1229.
731 **Uemura, T., Nakano, R.T., Takagi, J., Wang, Y., Kramer, K., Finkemeier, I.,**
732 **Nakagami, H., Tsuda, K., Ueda, T., Schulze-Lefert, P., and Nakano, A.** A
733 golgi-released subpopulation of the trans-golgi network mediates protein secretion
734 in arabidopsis 1. Plant Physiol. 2019:**179**: 519–532.
735 **Vaddepalli, P., Fulton, L., Wieland, J., Wassmer, K., Schaeffer, M., Ranf, S., and**

736 **Schneitz, K.** The cell wall-localized atypical β-1,3 glucanase ZERZAUST controls
737 tissue morphogenesis in Arabidopsis thaliana. Dev. 2017:**144**: 2259–2269.
738 **Wang, X., Chung, K.P., Lin, W., and Jiang, L.** Protein secretion in plants:
739 Conventional and unconventional pathways and new techniques. J. Exp. Bot.
740 2017:**69**: 21–37.
741 **Zavaliev, R., Dong, X., and Epel, B.L.** Glycosylphosphatidylinositol (GPI)
742 modification serves as a primary plasmodesmal sorting signal. Plant Physiol.
743 2016:**172**: 1061–1073.
744

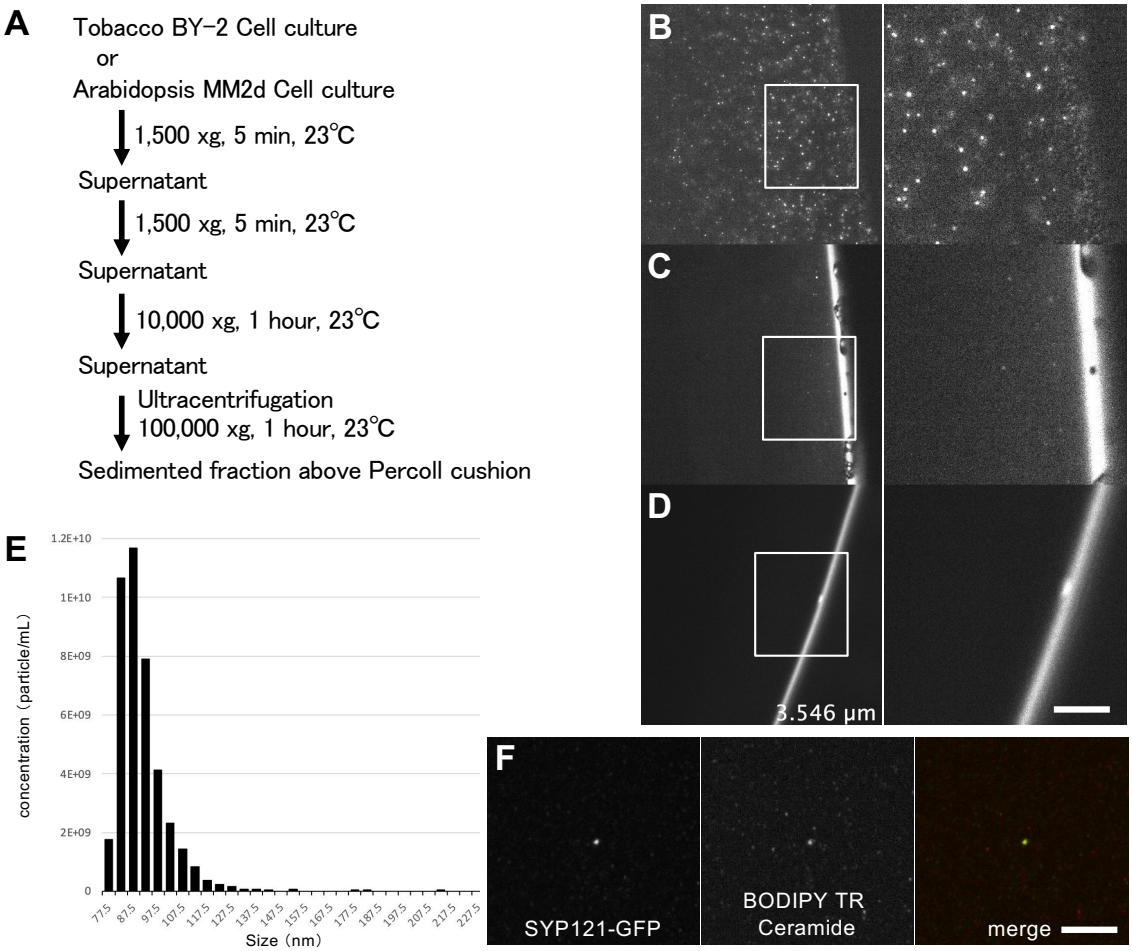

Figure 1. Isolation of EVs from a plant cell culture suspension

A) Protocol for the isolation of EVs from plant cell cultures. **B–D)** BODIPY TR Ceramide staining of the ultracentrifugation-derived sedimented fraction (B) and supernatant fraction (C) for the tobacco BY-2 culture medium and the ultracentrifugation-derived sedimented fraction for the medium before culturing (D). The panels on the right present the enlarged images of the area marked by a white square in the panels on the left. These images correspond to the optical section presented in Supplemental Movie 1. Bar, 2 μm. **E)** Size distribution of sedimented particles by ultracentrifugation from the supernatant of Arabidopsis MM2d cells. **F)** Purified EVs from SYP121-GFP transgenic tobacco BY-2 cell cultures. Bar, 2 μm.

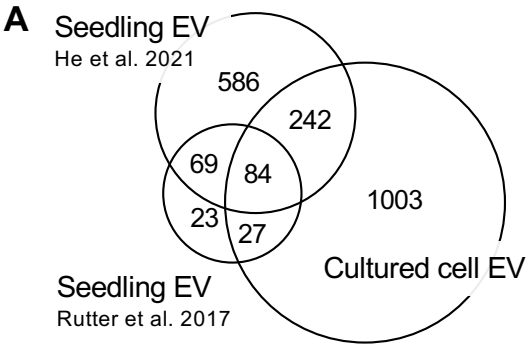

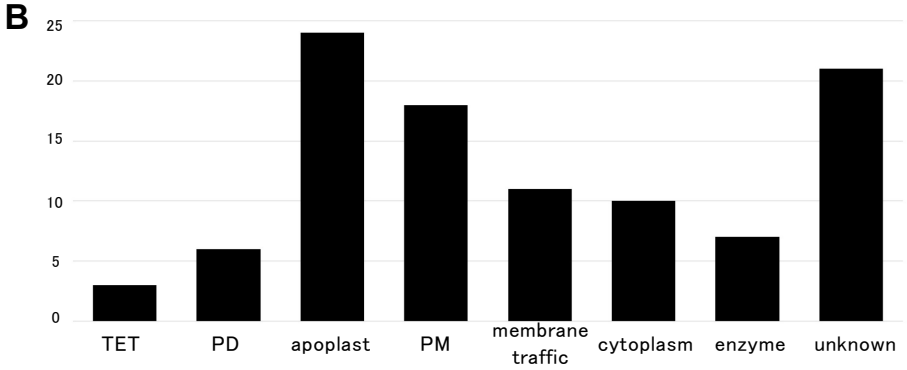

C

AGI code	Protein ID	Cultured cell EV this study	Seedling EV Rutter et al. 2017	Seedling EV He et al. 2021
AT5G46700	TET1,TRN2	*	N.D.	N.D.
AT2G19580	TET2	*	N.D.	N.D.
AT3G45600	TET3	*	N.D.	N.D.
AT5G60220	TET4	N.D.	N.D.	N.D.
AT4G23410	TET5	*	N.D.	N.D.
AT3G12090	TET6	N.D.	N.D.	N.D.
AT4G28050	TET7	*	N.D.	N.D.
AT2G23810	TET8	*	*	*
AT4G30430	TET9	*	N.D.	N.D.
AT1G63260	TET10	*	N.D.	N.D.
AT1G18520	TET11	N.D.	N.D.	N.D.
AT5G23030	TET12	N.D.	N.D.	N.D.
AT2G03840	TET13	N.D.	N.D.	N.D.
AT2G01960	TET14	N.D.	N.D.	N.D.
AT5G57810	TET15	N.D.	N.D.	N.D.
AT1G18510	TET16	N.D.	N.D.	N.D.
AT1G74045	TET17	N.D.	N.D.	N.D.

D

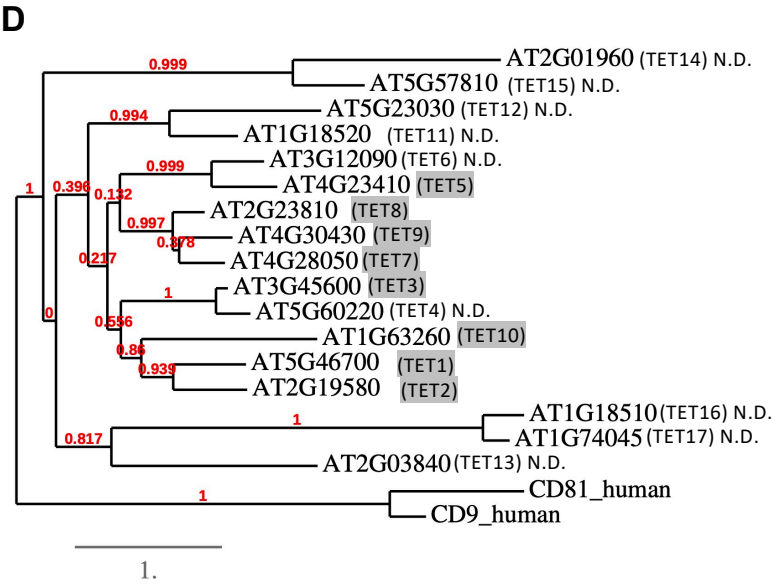

E

AGI code		Protein ID	Cultured cell EV this study	Seedling EV Rutter et al. 2017	Seedling EV He et al. 2021
AT3G11820	Qa-SNAREs	SYP121/SYR1	*	N.D.	*
AT3G52400	Qa-SNAREs	SYP122	*	*	*
AT4G03330	Qa-SNAREs	SYP123	N.D.	*	N.D.
AT1G61290	Qa-SNAREs	SYP124	N.D.	N.D.	N.D.
AT1G11250	Qa-SNAREs	SYP125	N.D.	N.D.	N.D.
AT3G03800	Qa-SNAREs	SYP131	N.D.	N.D.	N.D.
AT2G35190	Qb-SNAREs	NPSN11	*	N.D.	N.D.
AT1G48240	Qb-SNAREs	NPSN12	*	N.D.	*
AT3G17440	Qb-SNAREs	NPSN13	*	N.D.	*
AT1G04750	R-SNAREs	VAMP721	*	N.D.	*
AT2G33120	R-SNAREs	VAMP722	*	N.D.	*
AT2G33110	R-SNAREs	VAMP723	N.D.	N.D.	N.D.
AT4G15780	R-SNAREs	VAMP724	*	N.D.	N.D.
AT2G32670	R-SNAREs	VAMP725	N.D.	N.D.	N.D.
AT1G04760	R-SNAREs	VAMP726	N.D.	N.D.	N.D.
AT3G54300	R-SNAREs	VAMP727	N.D.	N.D.	N.D.
AT2G38410	ESCRT INTERACTORS	TOM1A	*	N.D.	N.D.
AT5G01760	ESCRT INTERACTORS	TOM1B	N.D.	N.D.	N.D.
AT1G76970	ESCRT INTERACTORS	TOM1C	N.D.	N.D.	N.D.
AT4G32760	ESCRT INTERACTORS	TOM1D	*	N.D.	N.D.
AT1G06210	ESCRT INTERACTORS	TOM1E	N.D.	N.D.	N.D.
AT1G21380	ESCRT INTERACTORS	TOM1F	*	N.D.	N.D.
AT5G16880	ESCRT INTERACTORS	TOM_L	*	N.D.	N.D.
AT5G63640	ESCRT INTERACTORS	TOM1G	*	N.D.	N.D.
AT3G08790	ESCRT INTERACTORS	TOM1H	N.D.	N.D.	N.D.

AGI code		Protein ID	Cultured cell EV this study	Seedling EV Rutter et al. 2017	Seedling EV He et al. 2021
AT3G12400	ESCRT-1	VPS23A	N.D.	N.D.	N.D.
AT5G13860	ESCRT-1	VPS23B	N.D.	N.D.	N.D.
AT4G05000	ESCRT-1	VPS28A	N.D.	N.D.	N.D.
AT4G21560	ESCRT-1	VPS28B	N.D.	N.D.	N.D.
AT3G53120	ESCRT-1	VPS37A	N.D.	N.D.	N.D.
AT2G36680	ESCRT-1	VPS37B	N.D.	N.D.	N.D.
AT4G27040	ESCRT-2	VPS22	N.D.	N.D.	N.D.
AT4G19003	ESCRT-2	VPS25	N.D.	N.D.	N.D.
AT5G04920	ESCRT-2	VPS36	N.D.	N.D.	N.D.
AT2G06530	ESCRT-3	CHMP2A	*	N.D.	N.D.
AT5G44560	ESCRT-3	CHMP2B	*	N.D.	N.D.
AT1G03950	ESCRT-3	CHMP2C	*	N.D.	N.D.
AT5G09260	ESCRT-3	VPS20A	*	N.D.	N.D.
AT5G63880	ESCRT-3	VPS20B	*	N.D.	N.D.
AT5G22950	ESCRT-3	VPS24A	*	N.D.	N.D.
AT3G45000	ESCRT-3	VPS24B	N.D.	N.D.	N.D.
AT2G19830	ESCRT-3	SNF7A	*	N.D.	N.D.
AT4G29160	ESCRT-3	SND7B	*	N.D.	N.D.
AT2G27600	ESCRT REGULATOR	VPS4	*	N.D.	N.D.
AT3G10640	ESCRT REGULATOR	VPS60A	*	N.D.	N.D.
AT5G04850	ESCRT REGULATOR	VPS60B	N.D.	N.D.	N.D.
AT1G73030	ESCRT REGULATOR	CHMP1A	*	N.D.	N.D.
AT1G17730	ESCRT REGULATOR	CHMP1B	N.D.	N.D.	N.D.
AT1G15130	ESCRT REGULATOR	BRO1	*	N.D.	*
AT4G26750	ESCRT REGULATOR	VTA1	N.D.	N.D.	N.D.

Figure 2. Comparison between the cell culture EV proteome and the seedling apoplast EV proteome
A) Venn diagram of the identified proteins in the cell culture EV proteome and the seedling apoplast EV proteome. **B)** Classification of the top 100 high-intensity proteins in the cell culture EV proteome. **C)** Identified tetraspanin family members in the cell culture EV proteome and the seedling apoplast EV proteome. **D)** Phylogenetic tree of the tetraspanin family in Arabidopsis thaliana. Identified tetraspanin family members in the cell culture EV proteome were colored in gray. **E)** Identified membrane trafficking proteins in the cell culture EV proteome and the seedling apoplast EV proteome.

A

AGI code	Name	Protein ID	**Cultured cell EV** this study	Category	**Seedling EV** Rutter et al. 2017	**Seedling EV** He et al. 2021	**PD** Fernandez-Calvino et al. 2011	**PD** Brault et al. 2019	**Apoplast** Uemura et al. 2019
AT5G61130	plasmodesmata callose-binding protein 1	PDCB1	*	PD	N.D.	N.D.	N.D.	*	*
AT1G69295	plasmodesmata callose-binding protein 4	PDCB4	*	PD	N.D.	N.D.	N.D.	*	*
AT5G06320	NDR1/HIN1-like 3	NHL3	*	Cytoplasm	*	*	*	*	N.D.
AT1G64760	O-Glycosyl hydrolases family 17 protein	1,3-beta-glucosidase	*	apoplast	N.D.	N.D.	*	*	N.D.
AT2G23810	tetraspanin8	TET8	*	TET	*	*	*	*	N.D.
AT4G31140	O-Glycosyl hydrolases family 17 protein	1,3-beta-glucosidase	*	apoplast	*	*	*	*	N.D.
AT5G43980	plasmodesmata-located protein 1	PDLP1	*	PD	N.D.	N.D.	*	*	*
AT1G74020	strictosidine synthase 2	SSL12	*	apoplast	N.D.	N.D.	*	N.D.	*
AT5G58090	O-Glycosyl hydrolases family 17 protein	1,3-beta-glucosidase	*	apoplast	*	*	*	*	*
AT4G12420	Cupredoxin superfamily protein	SKU5	*	apoplast	*	*	*	N.D.	*
AT3G25290	Auxin-responsive family protein	Cytochrome b561	*	PM	N.D.	N.D.	*	N.D.	N.D.
AT5G26340	Major facilitator superfamily protein	STP13	*	PM	*	*	*	N.D.	N.D.
AT5G08080	syntaxin of plants 132	SYP132	*	membrane traffic	*	*	*	N.D.	N.D.
AT3G52400	syntaxin of plants 122	SYP122	*	membrane traffic	*	*	*	N.D.	N.D.
AT5G46700	Tetraspanin family protein	TET1, TRN2	*	TET	N.D.	N.D.	*	*	N.D.
AT1G31340	related to ubiquitin 1	RUB1	*	Cytoplasm	N.D.	N.D.	N.D.	N.D.	N.D.
AT2G27260	Late embryogenesis abundant (LEA)	LEA	*	Cytoplasm	N.D.	N.D.	*	N.D.	N.D.
AT2G18960	H[+]-ATPase 1	AHA1	*	PM	*	*	*	N.D.	*
AT2G47170	Ras-related small GTP-binding family protein	ARF1	*	membrane traffic	N.D.	N.D.	*	N.D.	N.D.
AT4G25240	SKU5 similar 1	SKS1	*	apoplast	N.D.	N.D.	*	*	*
AT5G25460	transmembrane protein 2C putative	DGR2	*	PM	N.D.	*	*	N.D.	*
AT2G16600	rotamase CYP 3	CYP19-1	*	Cytoplasm	*	N.D.	*	N.D.	N.D.
AT3G52470	Late embryogenesis abundant (LEA)	LEA	*	Cytoplasm	N.D.	N.D.	*	*	N.D.
AT5G42980	thioredoxin 3	TRX3	*	enzyme	*	N.D.	*	N.D.	N.D.
AT2G44790	uclacyanin 2	uclacyanin 2	*	apoplast	*	N.D.	*	N.D.	*
AT1G74010	Calcium-dependent phosphotriesterase	phosphotriesterase	*	enzyme	N.D.	N.D.	N.D.	*	N.D.
AT2G16060	hemoglobin 1	AHB1	*	apoplast	N.D.	N.D.	*	N.D.	N.D.
AT5G19390	Rho GTPase activation protein (RhoGAP)	ROPGAP7	*	membrane traffic	N.D.	N.D.	N.D.	N.D.	N.D.
AT3G11820	syntaxin of plants 121	SYP121	*	membrane traffic	*	*	*	N.D.	N.D.
AT3G02740	Eukaryotic aspartyl protease family protein	aspartyl protease	*	apoplast	*	N.D.	N.D.	N.D.	*

B

	Number of Identified proteins	Cultured cell EV	Seedling EV Rutter et al. 2017	Seedling EV He et al. 2021	Plasmodesmata Fernandez et al. 2011	Plasmodesmata Brault et al. 2019	Apoplast Uemura et al. 2019
Cultured cell EV	1356	N. A.	8.2% (111/1356)	24.1% (326/1356)	23.5% (318/1356)	5.7% (77/1356)	44.6% (604/1356)
Seedling EV Rutter et al. 2017	204	54.5% (111/204)	N. A.	75% (153/204)	55.4% (113/204)	3% (6/204)	66.7% (136/204)
Seedling EV He et al. 2021	981	33.3% (326/981)	15.6% (153/981)	N. A.	37.7% (370/981)	1.8% (17/981)	55% (539/981)
Plasmodesmata Fernandez-Calvino et al. 2011	1260	25.2% (318/1260)	9% (113/1260)	29.4% (370/1260)	N. A.	4.8% (61/1260)	41.0% (517/1260)
Plasmodesmata Brault et al. 2019	115	67% (77/115)	5.3% (6/115)	14.8% (17/115)	53% (61/115)	N. A.	30.5% (35/115)
Apoplast Uemura et al. 2019	3219	18.8% (604/3219)	4.3% (136/3219)	16.8% (539/3219)	16.1% (517/3219)	1.1% (35/3219)	N. A.

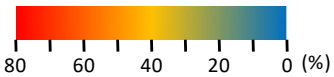

Figure 3. Comparison between the EV proteome and the plasmodesmata proteome
A) Comparison of the EV proteomes and the plasmodesmata proteomes in terms of the top 30 high-intensity proteins in the cell culture EV proteomes. **B)** Overlap percentages between the three EV proteomes and the two plasmodesmata proteomes. The EV and plasmodesmata fractions were indistinguishable in these analyses.

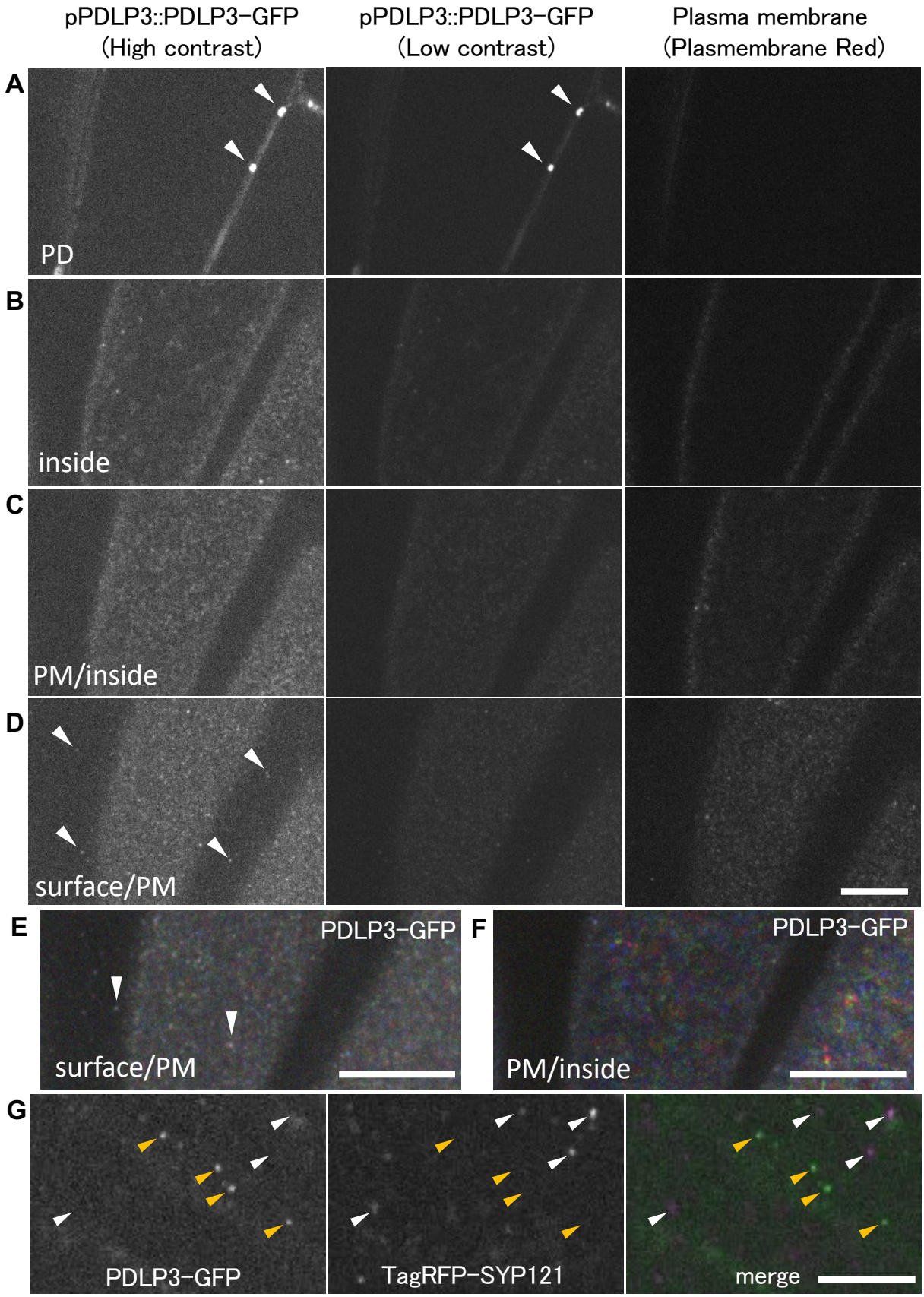

Figure 4. Localization of PDLP3-GFP in the apoplast region

A-D) Confocal microscopy images of PDLP3-GFP. Plasma membrane was labeled by Plasmembrane Red. PDLP3-GFP clearly localized to plasmodesmata (**A**, white arrowheads). At high contrast images, the PDLP3-GFP signals were also observed as particles at inside (**B**), plasma membrane (**C**), and surface (**D**). Some PDLP3-GFP signals were detected as small particles in the apoplast region (**D**, white arrowheads). Bar, 10 μm.

E, F) Projection images from PDLP3-GFP time-lapse analyses. The 15 time-lapse images were acquired every 5 seconds and grouped into early (1-5), middle (6-10), and late (11-15) phases. These images were projected at maximum intensity, and superimposed into one merge image using blue, green and red colour, respectively. Bars, 10 μm. **G)** Comparison of PDLP3-GFP and TagRFP-SYP121 at the apoplast region. TagRFP-SYP121 (white arrowheads) were not colocalized with PDLP3-GFP (yellow arrowheads). Bar, 5 μm.

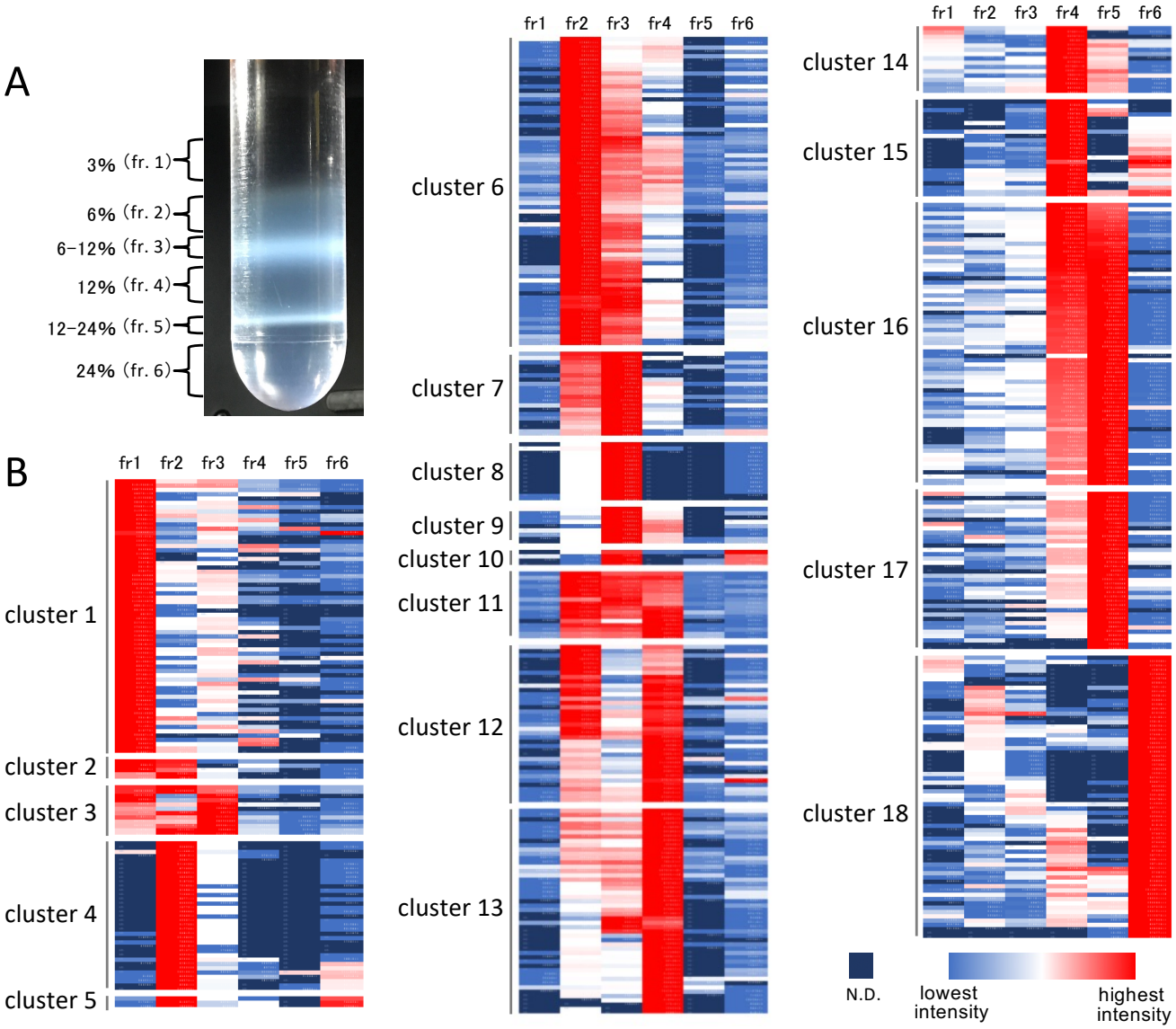

Figure 5. Iodixanol density gradient ultracentrifugation of the crude EV fraction

A) Separation of the crude EV fraction by an iodixanol density gradient ultracentrifugation. The crude EV fraction was mounted on the top of the iodixanol solution during the density gradient ultracentrifugation (24%, 12%, 6%, and 3% iodixanol solutions). After the ultracentrifugation, six fractions were recovered and used for proteome analyses. **B)** Classification of the 524 identified proteins on the basis of their distribution. The presented data correspond to the information provided in Supplemental Table 5.

A

AGI code	Protein ID	cl.	cat.	fr.1	fr.2	fr.3	fr.4	fr.5	fr.6
AT5G46700	TET1,TRN2	12	EV	3E+07	6E+07	5E+07	7E+07	5E+07	7E+07
AT2G23810	TET8	12	EV	4E+08	7E+08	4E+08	1E+09	6E+08	3E+08
AT3G45600	TET3	13	EV	6E+06	2E+07	2E+07	4E+07	1E+07	8E+06
AT2G19580	TET2	12	EV	9E+06	2E+07	1E+07	2E+07	N.D.	8E+06
AT4G30430	TET9	12	EV	5E+06	3E+07	7E+06	2E+07	5E+06	2E+06
AT3G11820	SYP121	11	EV	2E+07	1E+08	9E+07	1E+08	5E+06	2E+07
AT3G52400	SYP122	12	EV	5E+07	2E+08	1E+08	7E+08	2E+07	1E+08
AT5G08080	SYP132	12	EV	4E+07	2E+08	1E+08	3E+08	4E+07	8E+07
AT1G04750	VAMP721	13	EV	1E+07	5E+07	5E+07	8E+07	1E+07	3E+07
AT4G15780	VAMP724	13	EV	N.D.	N.D.	1E+06	2E+06	N.D.	8E+05
AT5G58060	YKT61	13	EV	N.D.	9E+06	1E+07	1E+07	1E+06	3E+06

B

AGI code	Protein ID	cl.	cat.	fr.1	fr.2	fr.3	fr.4	fr.5	fr.6
AT5G43980	PLDP1	6	PD	2E+08	6E+08	4E+08	5E+08	3E+08	4E+08
AT2G33330	PLDP3	6	PD	1E+07	4E+07	2E+07	2E+07	1E+06	2E+07
AT2G01660	PLDP6	6	PD	2E+07	6E+07	5E+07	5E+07	3E+06	3E+07
AT1G69295	PDCB4	6	PD	4E+08	1E+09	1E+09	8E+08	2E+08	1E+08
AT3G58100	PDCB5	7	PD	6E+06	4E+07	6E+07	2E+07	N.D.	3E+06
AT5G61130	PDCB1	6	PD	3E+08	2E+09	1E+09	1E+09	3E+08	7E+07

C

AGI code	Protein ID	cl.	cat.	fr.1	fr.2	fr.3	fr.4	fr.5	fr.6
AT2G35190	NPSN11	18	other	5E+05	2E+06	1E+06	2E+06	1E+06	4E+06
AT3G17440	NPSN13	4	PD	N.D.	2E+07	9E+06	5E+06	N.D.	1E+07
AT3G09740	SYP71	18	other	N.D.	7E+05	8E+05	3E+06	4E+06	1E+07
AT2G06530	CHMP2A	12	EV	2E+06	5E+07	4E+07	9E+07	3E+06	5E+06
AT5G44560	CHMP2B	7	PD	N.D.	4E+06	4E+06	3E+06	N.D.	5E+05
AT5G63880	VPS20B	4	PD	N.D.	4E+06	3E+06	N.D.	N.D.	4E+05
AT5G22950	VPS24A	13	EV	3E+06	3E+07	3E+07	3E+07	N.D.	2E+06
AT2G19830	SNF7A	4	PD	N.D.	5E+06	9E+05	N.D.	N.D.	N.D.
AT1G73030	CHMP1A	4	PD	N.D.	5E+06	3E+06	N.D.	N.D.	5E+05
AT1G32050	SCAMP5	12	EV	2E+07	6E+07	2E+07	7E+07	8E+06	2E+07
AT1G61250	SCAMP1	11	EV	2E+07	1E+08	1E+08	8E+07	2E+07	3E+07
AT1G11180	SCAMP2	4	PD	N.D.	7E+06	5E+06	N.D.	N.D.	5E+05
AT2G20840	SCAMP3	6	PD	2E+06	1E+07	5E+06	6E+06	N.D.	2E+06

D

AGI code	Protein ID	cl.	cat.	fr.1	fr.2	fr.3	fr.4	fr.5	fr.6
AT5G02290	oligopeptide transporter 3	6	PD	N.D.	3E+06	2E+06	2E+06	N.D.	1E+06
AT3G54140	peptide transporter 1(PTR1)	6	PD	9E+06	7E+07	6E+07	6E+07	3E+07	5E+07
AT3G15380	PM choline transporter	6	PD	2E+06	2E+07	2E+07	1E+07	3E+06	2E+06
AT4G16480	inositol transporter 4(INT4)	4	PD	N.D.	1E+07	8E+06	N.D.	3E+06	8E+06
AT1G16890	PUT4	4	PD	N.D.	2E+06	1E+06	N.D.	N.D.	N.D.
AT5G01240	LAX1	4	PD	N.D.	3E+06	3E+06	N.D.	N.D.	2E+06
AT1G11260	sugar transporter 1(STP1)	6	PD	4E+06	4E+07	4E+07	3E+07	N.D.	2E+07
AT3G19930	sugar transporter 4(STP4)	15	EV	N.D.	8E+06	7E+06	1E+07	N.D.	8E+06
AT3G53420	sugar transporter 7	15	EV	N.D.	3E+06	4E+06	1E+07	N.D.	5E+06
AT2G38940	phosphate transporter 1;4	12	EV	N.D.	1E+07	1E+07	2E+07	4E+06	3E+06
AT1G60030	NAT7	15	EV	N.D.	6E+06	6E+06	2E+07	8E+06	1E+07
AT1G69850	nitrate transporter 1:2	18	other	N.D.	1E+06	5E+05	2E+06	N.D.	3E+06
AT2G27810	NAT12	18	other	N.D.	2E+06	5E+05	3E+06	N.D.	6E+06
AT2G18960	H[+]-ATPase 1	18	other	2E+07	3E+07	1E+07	2E+08	2E+08	8E+08
AT4G30190	H[+]-ATPase 2	18	other	N.D.	3E+06	3E+06	1E+07	3E+07	1E+08
AT1G73590	PIN1	18	other	N.D.	4E+06	5E+06	7E+06	4E+06	2E+07
AT1G70940	PIN3	18	other	N.D.	6E+06	4E+06	5E+06	5E+06	2E+07

E

AGI code	Protein ID	cl.	cat.	fr.1	fr.2	fr.3	fr.4	fr.5	fr.6
AT3G11650	NDR1/HIN1-like 2	12	EV	4E+07	6E+07	4E+07	5E+07	2E+07	2E+07
AT5G06320	NDR1/HIN1-like 3	11	EV	7E+08	1E+09	1E+09	1E+09	5E+08	4E+08
AT2G27080	NDR1/HIN1-like 13	14	EV	6E+06	6E+06	8E+06	2E+07	1E+07	5E+06
AT2G35980	YLS9	14	EV	2E+07	6E+06	5E+06	4E+07	2E+07	1E+07
AT5G22200	HIN1 family protein	15	EV	3E+06	2E+07	1E+07	2E+07	N.D.	2E+07
AT1G06700	PTI1-1	12	EV	5E+06	5E+07	4E+07	6E+07	4E+06	3E+07
AT2G30740	PTI1-2	13	EV	3E+06	6E+07	7E+07	9E+07	5E+06	3E+07
AT2G47060	PTI1-4	13	EV	3E+06	3E+07	3E+07	4E+07	N.D.	1E+07

F

AGI code	Protein ID	cl.	cat.	fr.1	fr.2	fr.3	fr.4	fr.5	fr.6
AT4G25240	SKS1	13	EV	6E+07	1E+08	1E+08	2E+08	2E+07	2E+07
AT1G55570	SKS12	16	other	5E+08	7E+08	8E+08	4E+09	5E+09	6E+07
AT5G51480	SKS2	1	other	7E+07	4E+07	4E+07	5E+07	4E+07	2E+07
AT5G48450	SKS3	6	PD	6E+06	2E+07	2E+07	1E+07	4E+06	9E+06
AT1G76160	SKS5	16	other	5E+09	7E+09	6E+09	5E+10	6E+10	3E+09
AT4G12420	SKU5	16	other	2E+07	6E+07	6E+07	2E+08	1E+08	3E+07
AT5G21105	Plant L-ascorbate oxidase	16	other	3E+08	4E+08	5E+08	4E+09	5E+09	2E+08
AT3G43670	Copper amine oxidase family	14	EV	8E+06	5E+06	9E+06	6E+07	1E+07	N.D.
AT1G62810	Copper amine oxidase family	15	EV	2E+06	N.D.	3E+06	1E+07	8E+06	N.D.
AT1G51540	Galactose oxidase	16	other	2E+08	2E+08	2E+08	2E+09	2E+09	4E+07
AT3G27220	Galactose oxidase	16	other	9E+07	2E+08	2E+08	2E+09	2E+09	6E+07
AT3G63080	glutathione peroxidase 5	12	EV	3E+06	2E+07	2E+07	3E+07	5E+06	1E+07
AT1G68220	aerobic coproporphyrinogen-III oxidase (DUF1218)	6	PD	1E+07	9E+07	9E+07	4E+07	7E+06	1E+07
AT5G11540	D-arabinono-1,4-lactone oxidase	3	other	7E+07	1E+08	1E+08	1E+07	9E+06	1E+07
AT5G06720	peroxidase 2	1	other	1E+09	7E+07	2E+08	N.D.	N.D.	N.D.
AT2G22420	Peroxidase family	1	other	2E+08	1E+07	2E+07	4E+06	N.D.	1E+06
AT2G41480	Peroxidase family	6	PD	7E+06	3E+07	2E+07	1E+07	4E+06	3E+06
AT2G37130	Peroxidase family	14	EV	4E+07	3E+07	4E+07	4E+08	1E+08	5E+06
AT4G08770	Peroxidase family	16	other	1E+07	1E+07	1E+07	5E+08	8E+08	7E+06
AT5G58390	Peroxidase family	17	other	N.D.	N.D.	N.D.	1E+08	2E+08	1E+06
AT5G64120	Peroxidase family	17	other	9E+06	3E+06	4E+06	2E+07	4E+07	N.D.
AT5G05340	Peroxidase family	17	other	1E+08	3E+08	3E+08	3E+09	8E+09	4E+08
AT3G49120	peroxidase CB	16	other	N.D.	1E+06	2E+06	4E+07	7E+07	4E+05

G

AGI code	Protein ID	cl.	cat.	fr.1	fr.2	fr.3	fr.4	fr.5	fr.6
AT4G29360	O-Glycosyl hydrolases	18	other	7E+06	7E+06	8E+06	2E+07	9E+06	2E+07
AT5G56590	O-Glycosyl hydrolases	11	EV	2E+07	7E+07	7E+07	9E+07	3E+07	7E+06
AT1G64760	ZET	13	EV	4E+08	9E+08	1E+09	1E+09	1E+08	8E+07
AT4G31140	O-Glycosyl hydrolases	13	EV	9E+07	3E+08	3E+08	5E+08	1E+08	4E+07
AT5G58090	O-Glycosyl hydrolases	13	EV	5E+07	6E+07	7E+07	7E+08	6E+07	1E+07
AT3G04010	O-Glycosyl hydrolases	7	PD	8E+06	2E+07	2E+07	9E+06	N.D.	4E+05
AT2G01630	PdBG2	6	PD	4E+07	1E+08	6E+07	6E+07	1E+06	8E+06
AT3G13560	PdBG1	1	other	2E+07	2E+07	1E+07	N.D.	N.D.	2E+06
AT1G66250	PdBG3	1	other	1E+07	5E+06	5E+06	9E+06	N.D.	5E+05
AT5G55180	O-Glycosyl hydrolases	1	other	3E+07	2E+06	7E+06	N.D.	N.D.	1E+06
AT5G42100	BG_pap	18	other	5E+06	3E+06	4E+06	2E+06	N.D.	1E+07
AT5G42720	O-Glycosyl hydrolases	1	other	5E+07	4E+06	1E+07	9E+06	N.D.	1E+07
AT4G34480	O-Glycosyl hydrolases	1	other	3E+09	2E+08	4E+08	6E+07	2E+07	8E+07

N.D. lowest intensity highest intensity

Figure 6. Representative proteins in each gene ontology category

A) Representative EV proteins. B) Representative PD proteins. C) Membrane trafficking-related proteins. D) Membrane transporters and pumps. E) Disease resistance-related proteins. F) Oxidases and peroxidases. G) O-glycosyl hydrolases. The presented data correspond to the information provided in Supplemental Table 5. cl. indicates the cluster number in Figure 5B; cat. indicates category.

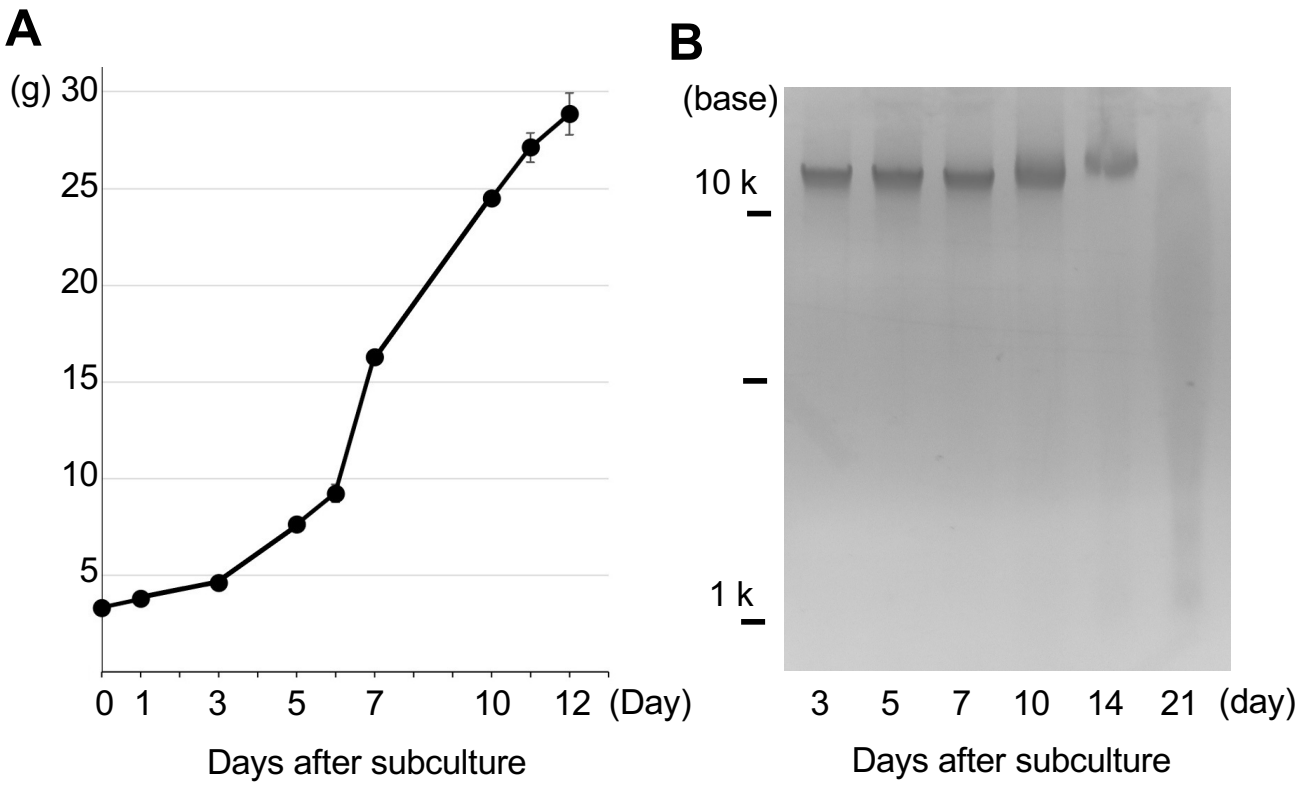

Supplemental Figure 1. Growth condition of MM2d Arabidopsis cultured cells for this study

A) Growth curve of MM2d Arabidopsis cultured cells in this study. Supernatant of 5 days-old and 7 days-old cultured cells was applied for EV purification. **B)** DNA degradation assay of MM2d cells. In 5 days-old and 7 days-old cultured cells, DNA degradation did not occur at all.

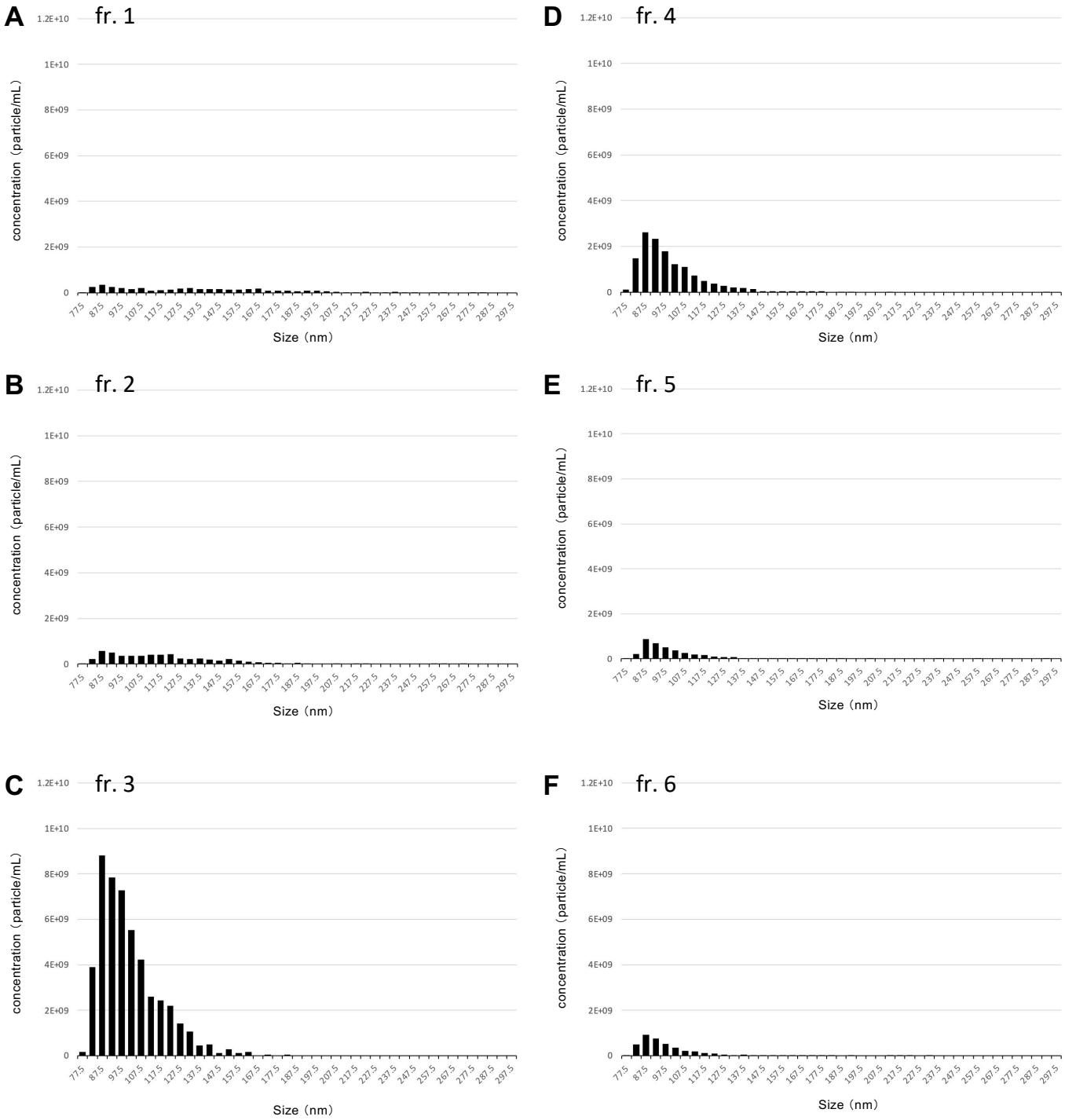

Supplemental Figure 2. Size distribution of EVs in each fraction after an iodixanol density gradient ultracentrifugation.

Six fractions were recovered after an iodixanol density gradient ultracentrifugation and used for size distribution analyses. These fractions correspond to the fractions in Figure 5A.